International Journal of Coal Geology 257 (2022) 104012

Contents lists available at ScienceDirect

International Journal of Coal Geology

journal homepage: www.elsevier.com/locate/coal

Differences and origins of hydrocarbon generation characteristics between mudstone and shale in the Seventh Member of the Yanchang Formation, Ordos Basin, China

Ruihui Zheng [a,b], Yifan Wang [a,b], Zhipeng Li [a,b], Zhihuan Zhang [a,b,*], Guangli Wang [a,b], Heng Zhang [c]

[a] College of Geosciences, China University of Petroleum, Beijing 102249, China
[b] State Key Laboratory of Petroleum Resources and Prospecting, China University of Petroleum, Beijing 102249, China
[c] The Fifth Oil Production Plant of Changqing Oilfiled Company, Xi'an, Shaanxi 710000, China

ARTICLE INFO

Keywords:
Shale and mudstone
Geochemistry characteristics
Hydrocarbon generation process
Seventh Member of the Yanchang Formation
Ordos Basin

ABSTRACT

Organic-rich black shale and dark-grey mudstone are widespread in the Seventh Member of the Yanchang Formation, Ordos Basin. There are obviously differences in geochemical characteristics and hydrocarbon generation potential between black shale and dark-grey mudstone. Based on the detailed organic geochemical examination, this paper reveals the differences in hydrocarbon generation processes and characteristics (activation energy and conversion rate of hydrocarbon generation) between dark-grey mudstone and black shale and the causes for the differences. Black shale is characterized by moderate to very high total organic carbon (TOC) contents (5.08%–39.39%) and its kerogen type belongs to type II_1 and type I. Dark-grey mudstone has a characteristic of low to moderate TOC contents (0.64%–7.35%) and its kerogen types are mainly composed of type II_2 and type II_1. The hydrocarbon generation activation energy of black shale mainly oscillates around 250–310 KJ/mol, and the corresponding hydrocarbon generation threshold is high (the simulated temperature is 400 °C). The process of hydrocarbon generation is characterized by fast conversion rate and short cycle. By contrast, the hydrocarbon generation activation energy of dark-grey mudstone has a wide range (170–360 KJ/mol), and the corresponding hydrocarbon generation threshold is low (the simulated temperature is 230 °C). The process of hydrocarbon generation is characterized by slow conversion rate and long cycle. The difference of hydrocarbon generation process and characteristics between black shale and dark-grey mudstone is mainly affected by macerals composition and organic matter source. The organic matter of black shale mainly originated from algae, and its macerals was mainly composed of alginite. The organic matter of dark-grey mudstone mainly originated from the mixture of algae and terrestrial higher plants (conifers), and its macerals was mainly composed of vitrinite, liptodetrinite and inertinite. The complex macerals composition and organic matter source make the activation energy distribution of dark-grey mudstone more dispersed than that of black shale. In addition, affected by the macerals (e.g sporinite and resinite) with low activation energy from terrestrial higher plants, the activation energy of dark-grey mudstone containing sporinite and resinite in the macerals is lower than black shale. Therefore, the dark-grey mudstone containing algae and terrestrial higher plants corresponds to low hydrocarbon generation threshold, slow conversion rate and long hydrocarbon generation cycle. The black shale containing a large number of algae corresponds to high hydrocarbon generation threshold, fast conversion rate and short hydrocarbon generation cycle. Moreover, the conversion rate of black shale containing radioactive elements and more clay minerals is higher than that of dark-grey mudstone.

1. Introduction

Since exploration and production of shale oil made major breakthroughs in North America's marine strata (Soeder, 2018; Williams et al., 2021), Chinese geologists have also found abundant shale oil resources in continental strata of China and the shale oil production

* Corresponding author at: College of Geosciences, China University of Petroleum, Beijing 102249, China.
E-mail address: zhangzh3996@vip.163.com (Z. Zhang).

https://doi.org/10.1016/j.coal.2022.104012
Received 13 October 2021; Received in revised form 17 March 2022; Accepted 30 April 2022
Available online 2 May 2022

exceed 180 × 10^4 t in 2020 (Yang et al., 2016; Chen et al., 2018; Xi et al., 2020; Fu et al., 2020a; Li et al., 2021a, 2021b; Fu et al., 2021). Organic-rich sediments are not only important source rocks for conventional and unconventional reservoirs, but also can be the reservoirs themselves. With the breakthrough of shale oil exploration in the Seventh Member of the Triassic Yanchang Formation (Chang 7 Member) in the Qingcheng area, Ordos Basin (Fu et al., 2020b; Fu et al., 2021), research on organic-rich sediments of this member have received more and more attention (Li et al., 2020; Xi et al., 2020; Hou et al., 2021; Qiao et al., 2021; You et al., 2021). According to petrographic characteristics, two lithofacies of organic rich sediments are distinguished in the Chang 7 Member, namely dark-grey mudstone and black shale (Lin et al., 2017; Liu et al., 2018; Qi et al., 2019; Zhao et al., 2020; Fan et al., 2020; Qiao et al., 2021). Dark-grey mudstone is characterized by undeveloped lamellated structure and low to moderate organic matter abundance, while black shale has the characteristics of well-developed lamellated structure and high organic matter content (Lin et al., 2017; Liu et al., 2018; Fan et al., 2020; Zhao et al., 2020).

Source rocks are the material basis for petroleum systems, and their quality is affected by the supply, preservation condition, and dissolution of organic matter (Demaison and Moore, 1980; Arthur and Dean, 1998; Tyson, 2001; Rimmer et al., 2004; Lai et al., 2018; Sun et al., 2020; Hu et al., 2020). Different from those marine sedimentary basins, the supply and preservation condition of terrestrial sedimentary organic matter are easily affected by terrestrial organic matter input, seasonal climate change, and geology events, resulting in frequent changes of sedimentary cycles and strong heterogeneity of sediments. Therefore, the origin and preservation condition of organic matter are strongly affected by paleo-sedimentary environment in lacustrine sedimentary basins (Algeo et al., 2011; Wang et al., 2020; Chen et al., 2021a, 2021b).

The thermal maturity of organic matter also plays a vital role in evaluation of shale oil resources, which determines the conversion rate of organic matter (Yu et al., 2019; Leushina et al., 2021) and effects the distribution characteristics of shale oil (Yang et al., 2019). Theoretically, each type of chemical bond broken under thermal stress can be described with a group of kinetic parameters (frequency factor and activation energy), but due to the complexity of kerogen's chemical structure, a general kinetic model is usually used to describe the degradation process of kerogen (Wang et al., 2011). The information of the organic matter fractions can be obtained by the distribution characteristics of activation energy and frequency factor from the Arrhenius equation (Pepper and Corvit, 1995; Leushina et al., 2021). Generally, the kerogen fraction with low activation energy is firstly degraded, and the temperature (depth) corresponding to the oil generation window is relatively low (Leushina et al., 2021). Therefore, the differences of geochemical characteristics between dark-grey mudstone and black shale may lead to their differences in hydrocarbon generation kinetic characteristics.

There are abundant organic and inorganic compounds distributed in the strata, which play a very important role in hydrocarbon generation process. Some organic and inorganic compounds often participate in the evolution of organic matter as reactants and catalysts (Tissot, 1969; Johns and Shimoyama, 1972; Trent and George, 2002; Seewald, 2003). For example, clay minerals and some transition metal oxides can reduce the temperature of hydrocarbon generation (Mango, 2000), the increase of pressure can restrain the conversation of hydrocarbon (Uguna et al., 2012). Therefore, different lithologic source rocks containing different mineralogical composition may have different hydrocarbon generation processes (Chen et al., 2017). Previous studies have shown that there are obviously different in activation energy distribution and hydrocarbon generation conversion between dark-grey mudstone and black shale in the southern Ordos Basin (Huang et al., 2013; Qi et al., 2019). The distribution of activation energy of black shale is more concentrated than that of dark-grey mudstone in the southern Ordos Basin, which may be related to the difference of organic matter composition (Qi et al., 2019). These differences in chemical characteristics between dark-grey mudstone and black shale have significant impact on the formation and distribution of shale oil in the Ordos Basin, but there are few studies on their differences in hydrocarbon generation processes and characteristics and the reasons for the differences. It restricts the prediction of shale oil enrichment area. Furthermore, there is no systematic research on how the difference of hydrocarbon generation characteristics between the two types of source rocks affects the horizontal and vertical distribution of shale oil.

Through the comparison of hydrocarbon generation kinetics, organic matter abundance, macerals, and biomarkers composition, the differences in hydrocarbon generation processes and characteristics (activation energy and conversion rate of hydrocarbon generation) between dark-grey mudstone and black shale in the Chang 7 Member of Ordos Basin and the reasons for the differences are revealed. The research results are helpful to deeply understand their differences in resource potential and predict the shale oil enrichment areas, which provides a reference for the exploration of shale oil in the Chang 7 Member of Ordos Basin. In addition, the research results can also provide reference for the temperature setting of the in-situ conversion of low-medium mature shale in the Chang 7 Member of Ordos Basin.

2. Geological setting

Ordos Basin is located in North-Central China with an area of 37 × 10^4 km^2. It is the second largest sedimentary basin in China. The basin is surrounded by Yinshan Mountains in the north, Qinling Mountains in the south, Liupan Mountains and Helan Mountains in the west, and Luliang Mountains in the east, respectively. According to the current characteristics of geological structure and bedrock depth of the Odors Basin, the secondary tectonic units are divided into the northern Yimeng Uplift, the western Tianhuan Sag, the Western Thrust Belt, the central Yishan Slope, the eastern Jinxi Fold Belt, and the southern Weibei Uplift (Fig. 1). The Ordos Basin experienced six major tectonic-sedimentary evolution stages: 1) the formation period of crystalline basement in the Archeozoic – Early Proterozoic; 2) the formation period of aulacogen in the Middle – Late Proterozoic; 3) the formation period of marine carbonate platform in the Early Paleozoic; 4) the formation period of littoral plain in the Late Paleozoic; 5) the formation period of inland basin in the Mesozoic; 6) the formation period of peripheral faulted basin in the Cenozoic (Yang et al., 2005).

There are Mesoproterozoic and Lower Paleozoic marine source rocks, Upper Paleozoic marine-continental transitional source rocks, and Mesozoic lacustrine source rocks in Ordos Basin (Zhang et al., 2015; Liu et al., 2020; Chen et al., 2020; Zhao et al., 2021). The lacustrine sedimentary stratigraphic section of the Ordos Basin includes a series of formations with the age of Upper-Middle Triassic to Quaternary (Fig. 2a). The Upper-Middle Triassic strata contains Zhifang Formation and Yanchang Formation. The Yanchang Formation is divided into ten members (Fig. 2b), and it records the whole process of the paleo-lake from generation, development, prosperity to decline and disappear. During the deposition period of the Chang 7 Member, the area and depth of the paleo-lake are the largest. The Chang 7 Member is further subdivided into three layers (Chang 7^3, Chang 7^2, and Chang 7^1) from bottom to top (Fig. 2c). The Chang 7 Member is composed of sandstone, siltstone, muddy siltstone, silty mudstone, dark-grey mudstone, and black shale (Fig. 2c). From the plane distribution, dark-grey mudstone and black shale are complementary distributed along the northwest – southeast (Lin et al., 2017). Vertically, dark-grey mudstone is mostly interbedded with sandstone, with a thickness of 10–20 m, and mainly distributed in the Chang 7^1 and Chang 7^2. Black shale that is sandwiched between thinly bedded sandstone has a large thickness of 15–30 m, mainly located in the Chang 7^3 (Fig. 2c).

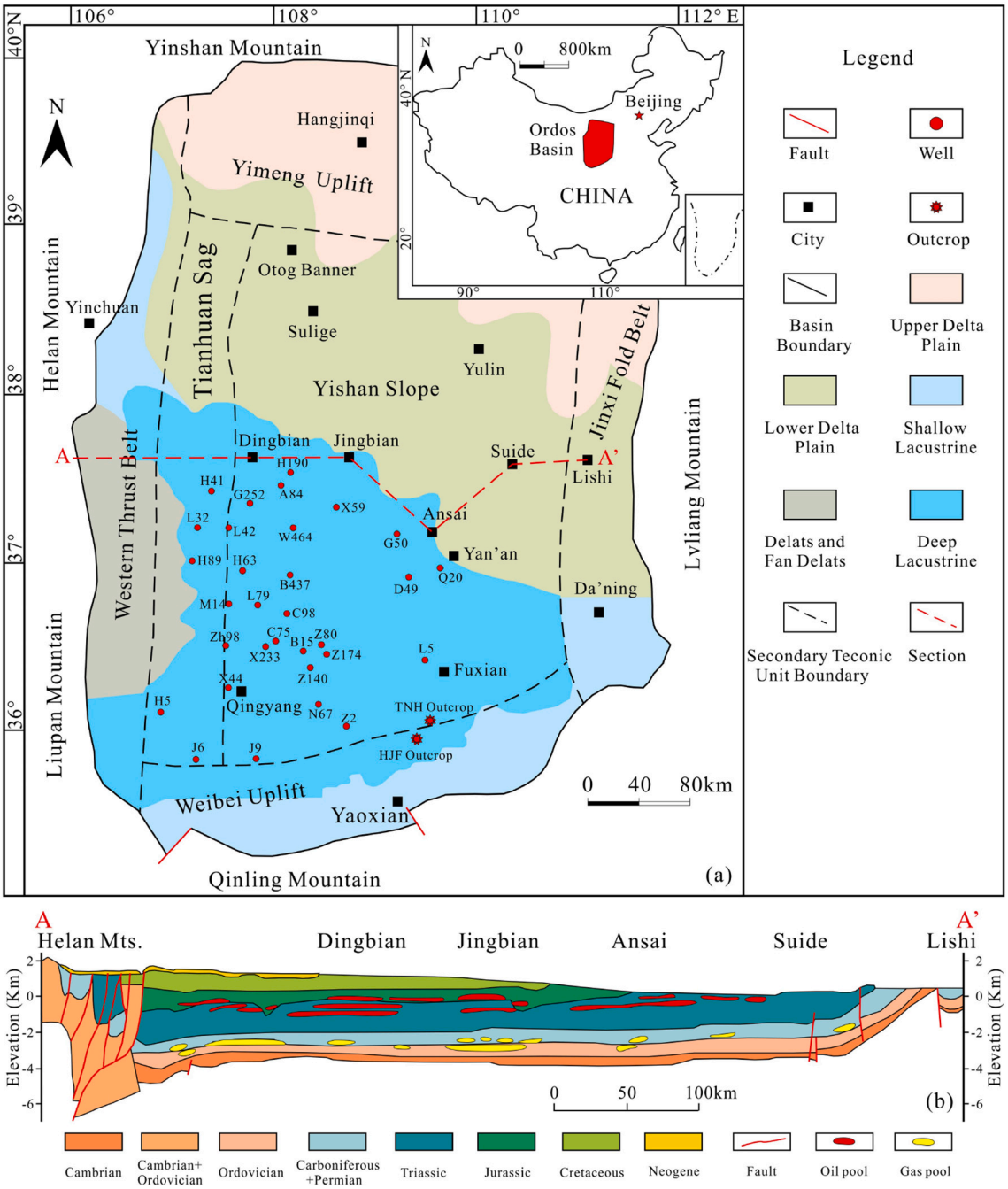

Fig. 1. Division of structural units, location of wells, and outcrops (from Chen et al., 2017; Fu et al., 2020a); (b) a geological cross section from west to east (from Yang et al., 2005) in the Ordos Basin.

3. Samples and methods

3.1. Samples collection and pretreatment

A total of 152 dark-grey mudstone and black shale core samples were collected from 30 wells in deep-water lacustrine facies of the Chang 7 Member in the Odors Basin. In addition, 23 black shale outcrop samples were collected from 2 field profiles in Tongchuan aera (Fig. 1). Among these samples, 10 low mature dark-grey mudstone and black shale were selected for kinetic simulation of hydrocarbon generation, 33 dark-grey mudstone and black shale with difference abundances were selected for biomarker and organic petrology analysis.

3.2. Total Organic carbon content and Rock-Eval pyrolysis

The dark-grey mudstone and black shale samples were crushed and sieved to 100 mesh. The dark-grey mudstone (100 mg) and black shale (10 mg) were treated by 5% HCl at 80 °C to remove inorganic carbon from samples, respectively. Then, these treated samples were washed with distilled water to fully remove the residual acid in the crucible, and these washed samples are dried in oven at 70 °C for 8 h. Finally, the iron powder and tungsten tin alloy were added to each sample as combustion improver, and the TOC contents of samples were detected on the LECO CS230 elemental analyzer.

The pyrolysis parameters of dark-grey mudstone and black shale were analyzed on the Rock-Eval II. The powder sample was first heated to 300 °C for 3 min to obtain the S_1 (free hydrocarbon), then continue

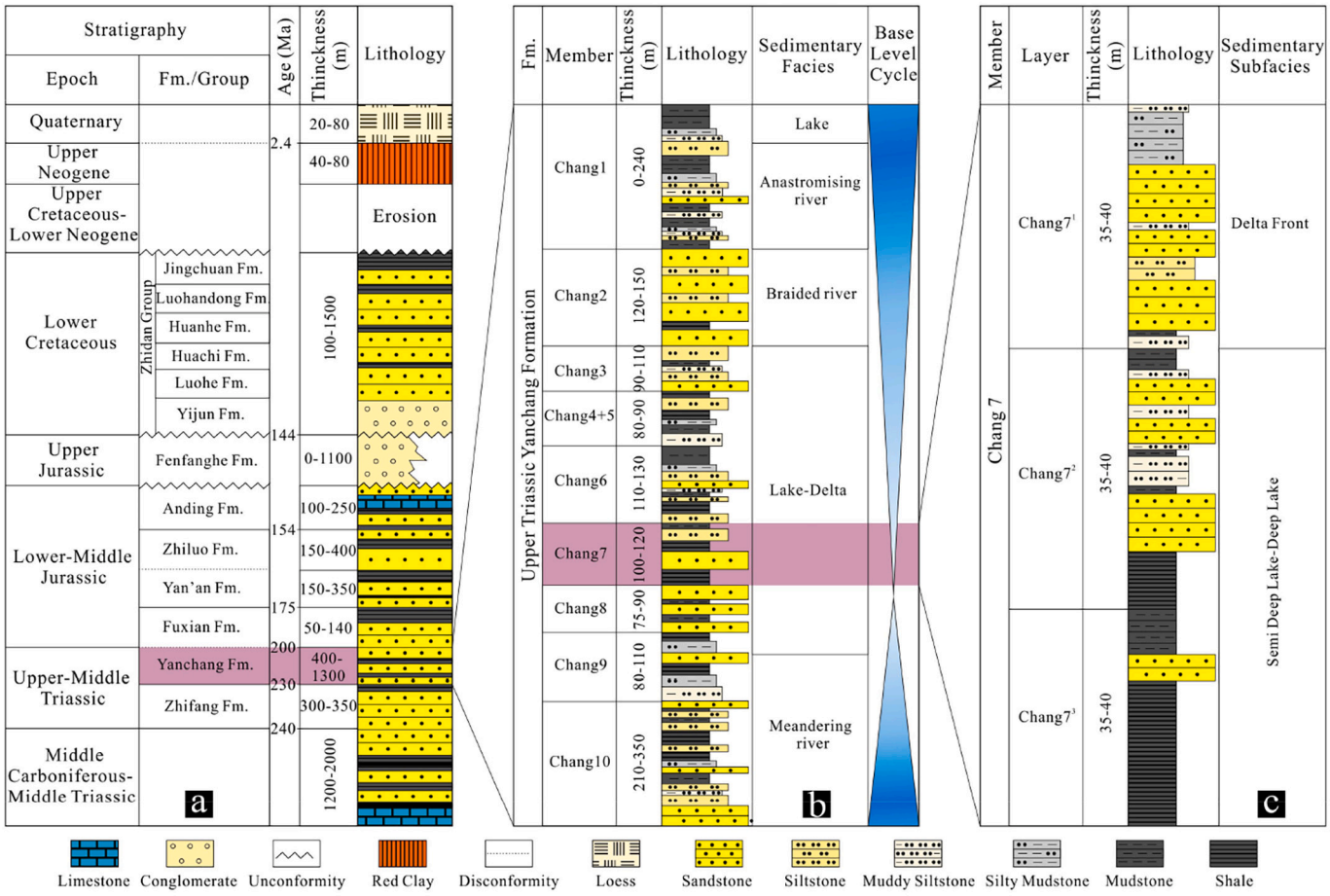

Fig. 2. Brief stratigraphic map of the Ordos Basin (a), stratigraphic division of the Yanchang Formation (b), and stratigraphic division of the Seventh Member of Yanchang Formation (c) (modified from Yang et al., 2010; Zhao et al., 2015).

heating to 600 °C at the rate of 25 °C/min to obtain the S_2 (pyrolysis hydrocarbon) and Tmax (highest pyrolysis peak temperature). Moreover, according to the above parameters, the hydrocarbon generation potential ($S_1 + S_2$, mg/g) and hydrogen index (HI = S_2/TOC, mg/g TOC) can be calculated.

3.3. Hydrocarbon generation kinetics

The kinetic simulation of hydrocarbon generation of dark-grey mudstone and black shale in the Chang 7 Member was carried out on the Rock-Eval II analyzer. The temperature program is as follows: first, the temperature was rapidly increased to 200 °C and lasts for 3 min to remove the free hydrocarbon in the sample. Then the sample was heated to 600 °C at the rates of 10 °C/min, 30 °C/min, 40 °C/min and 50 °C/min, respectively, and the hydrocarbon generation curves of the samples at different heating rates were obtained. Finally, according to the Arrhenius law (Pepper and Corvit, 1995), the frequency factor and activation energy of the sample can be calculated using the KINETICS 2015 software.

3.4. Organic petrology

The small bulk sample was mixed with epoxy resin to prepare a column with a diameter of 3.2 cm, and then the hardened column was cut and polished according to ISO 7404-2 (2009) to produce a highly reflective and scratch free surface. The maceral characteristics of dark-grey mudstone and black shale in the Chang 7 Member were observed on the Leica DM 4500P multipurpose microscope with 50-X oil immersion objective lens using reflected white light and ultraviolet fluorescence light. Before each vitrinite reflectance (Ro) measurement, a standard sample (Ro = 0.904%) was used to calibrate the instrument. The Ro value of sample represents the average value of at least 50 points, according to ISO 7404-5. Maceral composition and classification in source rocks were determined according to ICCP System 1994 (ICCP, 1998, 2001) and Pickel et al. (2017). Quantitative analysis of macerals was performed using a single scan method (Taylor et al., 1998), and at least 1000 points were counted for each polished block.

3.5. Molecular geochemistry

According to the TOC of samples, 60-70 g dark-grey mudstone and 30-40 g black shale were extracted by the Soxhlet extractor with dichloromethane for 24 h. Before extraction, copper foils were added to the flask to remove sulfur from the sample. Firstly, the asphaltene was filtered from extracts with petroleum ether. Then, the soluble fraction is separated into saturated, aromatic hydrocarbon and polar compounds through liquid- liquid phase separation (alumina: silica gel = 2:3). 30 mL petroleum ether was used to elute the saturated hydrocarbon, 20 mL mixture of dichloromethane and petroleum ether (2:1, v:v) was used to elute the aromatic hydrocarbon, and 10 mL dichloromethane was used to elute the polar compounds.

Gas chromatography–Mass spectrometry (GC–MS) analysis of saturated hydrocarbon was performed using the Agilent 5975i mass spectrometry, linked with the Agilent 6890 gas chromatography equipped with a 30 m × 0.25 mm i.d HP-5MS silica column (0.25 μm film thickness). Helium was used as the carrier gas with the average velocity of 36

cm/s. The initial temperature of the GC oven was set to 50 °C, then heated to 310 °C at the rate of 3 °C/min, and finally kept isothermal for 20 min. The ionization mode of electron impact is adopted, and the ionization energy is 70 eV.

The GC–MS analysis of aromatic hydrocarbon was performed using the Agilent 5975i mass spectrometry, linked with the Agilent 6890 gas chromatography equipped with a 60 m × 0.25 mm i.d HP-5MS silica column (0.25 μm film thickness). Helium was used as the carrier gas with the average velocity of 26 cm/s. The initial temperature of the GC oven was set to 80 °C, then heated to 310 °C at the rate of 3 °C/min, and finally keep isothermal for 20 min. The ionization mode of electron impact is adopted, and the ionization energy is 70 eV.

4. Results and discussion

4.1. Comparison of geochemical characteristics

The TOC and $S_1 + S_2$ values of dark-grey mudstone in the Chang 7 Member range from 0.64% to 7.35% (average: 3.39%) and 0.72 mg/g to 43.09 mg/g (average: 10.21 mg/g) (Fig. 3a), respectively. The HI and Tmax values of dark-grey mudstone in the Chang 7 Member range from 16.67 mg/g to 450.75 mg/g and 436 °C to 460 °C (Fig. 3b), respectively. The TOC and $S_1 + S_2$ values of black shale in the Chang 7 Member range from 5.08% to 39.39% (average: 16.10%) and 10.09 mg/g to 178.79 mg/g (average: 66.84 mg/g) (Fig. 3a), respectively. The HI and Tmax values of black shale in the Chang 7 Member range from 182.58 mg/g to 751.38 mg/g and 427 °C to 456 °C (Fig. 3b), respectively. The cross plot of HI and Tmax indicates that the kerogen type of dark-grey mudstone varies from type III to type II_1, and the kerogen type of black shale belongs to type II_1 and type I (Fig. 3b). Therefore, the dark-grey mudstone belongs to poor - very good source rock with high hydrocarbon generation potential, and black shale belongs to very good-excellent source rock with very high hydrocarbon generation potential. In addition, the Tmax values indicate a maturity of the dark-grey mudstone and black shale samples mainly within mature stage as seen in the Fig. 3b, except for the shale outcrop samples.

4.2. Comparison of characteristics of hydrocarbon generation kinetics

Based on the compensation relationship between temperature and time, the rapid heating in the laboratory can be used to simulate the hydrocarbon generation process of source rocks during geological burial. The hydrocarbon generation curves of source rocks under different geothermal gradients can be obtained by setting different heating rates. Owing to the pyrolysis process of type I and type II kerogen can be fully described by the parallel first-order reaction, the kinetics software can be used to obtain the best hydrocarbon generation path through fitting, and then the frequency factor (A) and activation energy (Ea) distribution of source rocks can be obtained (Schenk and Horsfield, 1998; Dieckmann et al., 2006; Mahlstedt et al., 2008). Kinetic

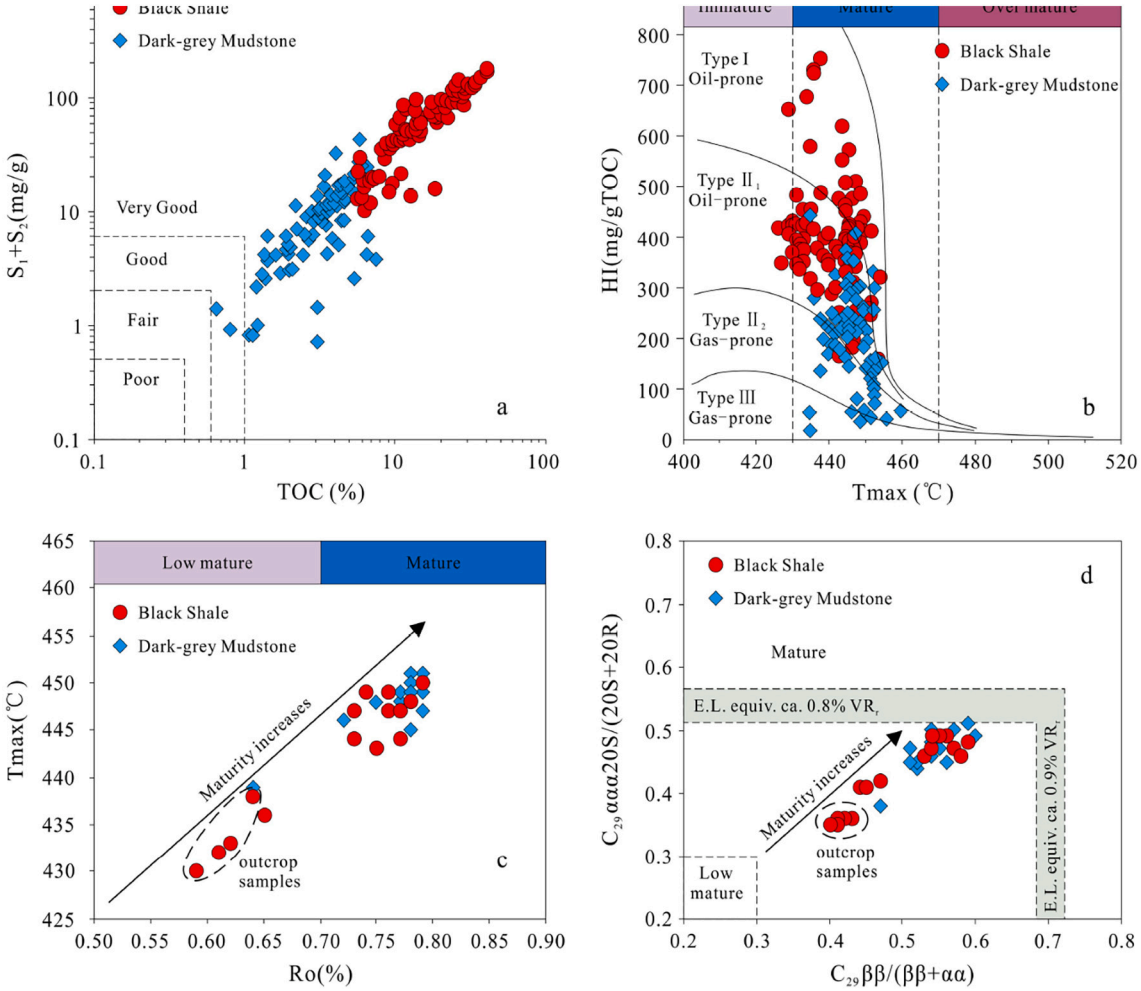

Fig. 3. Geochemical and biomarker parameters intersection diagram of dark-grey mudstone and black shale in the Seventh Member of Yanchang Formation. (a) $S_1 + S_2$ vs. TOC; (b) HI vs. Tmax; (c) Tmax vs. Ro; (d) C_{29} ααα20S/(20S + 20R) steranes vs. C_{29} ββ/(ββ + αα) steranes. E.L. equiv. = equilibration levels equivalent to vitrinite reflectance values (taken from Peters et al., 2005; George et al., 2001).

simulation results of dark-grey mudstone and black shale in the Chang 7 Member are shown in Fig. 4. There are obvious differences in activation energy distribution and hydrocarbon generation process between dark-grey mudstone and black shale.

The black shale of the Chang 7 Member is characterized by concentrated activation energy distribution, and the main activation energy ranges from 250 KJ/mol to 310 KJ/mol (Fig. 4a, c; Table 1), accounting for more than 85% of total. The corresponding frequent factors of the black shale range from 2.77E+10^{17} s^{-1} to 7.63E+10^{19} s^{-1}(Table 1). In contrast, the dark-grey mudstone of the Chang 7 Member is characterized by dispersed activation energy distribution, and the activation energy ranges from 170 KJ/mol to 360 KJ/mol, accounting for less than 70% of total (Fig. 4e, g; Table 1). The corresponding frequent factor of the dark-grey mudstone ranges from 3.22E+10^{14} s^{-1} and 2.83E+10^{23} s^{-1}(Table 1).

The standard deviation represents the deviation of the value from the average, so it can be used to describe the dispersion of a set of data. The higher the standard deviation of activation energy, the more dispersed the distribution of activation energy. The standard deviations of activation energy of black shale and dark-grey mudstone range from 17.91 KJ/mol to 28.93 KJ/mol and 24.27 KJ/mol to 37.52 KJ/mol (Table 1), respectively, which indicates that the activation energy distribution of dark-grey mudstone is more dispersed than that of black shale.

The conversion curves reveal the hydrocarbon generation characteristics of black shale and dark-grey mudstone in the Chang 7 Member (Fig. 4b, d, f, h). The simulated temperature of hydrocarbon generation is 400 °C at the beginning and 480 °C at the end, indicating that hydrocarbon generation of black shale occurs in a relatively narrow temperature range (≈80 °C). The simulated temperature of hydrocarbon generation is 230 °C at the beginning and 480 °C at the end, indicating that the hydrocarbon generation of dark-grey mudstone occurs in a relatively wide temperature range (≈250 °C).

Comparing the conversion curves of hydrocarbon generation between black shale and dark-grey mudstone, it shows that black shale has the characteristics of high hydrocarbon generation threshold, fast conversion rate and short hydrocarbon generation cycle, while dark-grey mudstone is characterized by low hydrocarbon generation threshold, slow conversion rate and long hydrocarbon generation cycle.

4.3. Mechanism analysis

Seventeen dark-grey mudstones and sixteen black shales are selected to analyze the causes of their differences in hydrocarbon generation characteristics (Fig. 1). The Ro values of selected dark-grey mudstone and black shale vary from 0.64% to 0.79% and 0.59% to 0.79% (Table 2). The Ro values indicate a maturity of the selected samples between the low maturity and early stage of maturity as seen in the Fig. 3c. Except for outcrop samples, the maturity of these source rock samples is basically close. Geochemical parameters of those samples are shown in Table 2.

4.3.1. Influence of organic petrological characteristics

The macerals of source rocks in the Chang 7 Member are mainly composed of liptinite, vitrinite and inertinite (Fig. 5a-c). Liptinite mainly contains alginite, sporinite, resinite and liptodetrinite (Fig. 5c-f). Vitrinite is dominated by telinite and vitrodetrinite, and the content of vitrinite in some samples is very high (Fig. 5b, c, f). Inertinite is mainly composed by fusinite and macrinite (Fig. 5b, f). The dark-grey mudstone and black shale in the Chang 7 Member have obvious differences in maceral composition (Fig. 6a). The macerals of dark-grey mudstone are dominated by liptinite, followed by vitrinite and inertinite, and the percentages of each component are 52.1%- 90.9%, 6.9%- 47.4% and 0.5–12.1% (Table 2), respectively. The macerals of black shale are dominated by liptinite, and the contents of other macerals are low (Fig. 6a). The percentages of liptinite, vitrinite and inertinite are 62.2%-97.0%, 1.7%- 36.8% and 0.4–8.7% (Table 2), respectively. Moreover, a large amount of pyrite is observed in black shale samples of the Chang 7 Member (Fig. 5f).

Previous studies shown that the distribution of activation energy of different macerals is different. For example, the activation energy of vitrinite and alginite are 160–350 KJ/mol and 220–270 KJ/mol (Sun et al., 1999; Jiang et al., 2005; Wang et al., 2017; Xu et al., 2018), respectively. The activation energy of fusinite in inertinite is widely distribution, ranging from 250 KJ/mol to 670 KJ/mol (Sun et al., 1999). Therefore, the dark-grey mudstone rich in vitrinite, liptodetrinite and inertinite has more dispersed distribution of activation energy, while the black shale rich in alginite has a more concentrated distribution of activation energy (Fig. 5 and Fig. 6a). The distribution of activation energy of dark-grey mudstone is more dispersed than that of black shale. In addition, there is a positive correlation between the standard deviation of activation energy and the ratio of (vitrinite + inertinite)/liptinite (Fig. 6b), indicating that the dispersed degree of activation energy increased with the increase of vitrinite and inertinite content. This further proves that the distribution characteristics of activation energy of source rocks is related to its maceral composition. The more complex maceral composition of source rocks, the more dispersed distribution of activation energy.

4.3.2. Influence of paleo-sedimentary environment and origin of organic matter

4.3.2.1. N-alkanes. The *n*-alkanes of dark-grey mudstone and black shale in the Chang 7 Member are characterized by unimodal distributions in these samples (Fig. 7a and b), but the proportion of low molecular weight *n*-alkanes in the black shale are relatively higher (Fig. 7b). The carbon number distribution of the *n*-alkanes may indicate the source of organic matter in low to medium maturity source rocks, the short-chain alkanes (nC_{15}, nC_{17}, nC_{19}) are considered to originate from algae and cyanobacteria, while the long-chain alkanes (nC_{27}, nC_{29}, nC_{31}) are considered to originate from waxes of higher plants (Gelpi et al., 1970; Killops and Killops, 2005). The (nC_{15}+ nC_{17}+ nC_{19})/ (nC_{27}+ nC_{29}+ nC_{31}) ratios of dark-grey mudstone and black shale range from 0.77 to 7.00 and 3.25 to 16.96 (Table 3), respectively. The ratio of (nC_{15}+ nC_{17}+ nC_{19})/ (nC_{27}+ nC_{29}+ nC_{31}) of black shale is higher than those of dark-grey mudstone under the condition of same thermal maturity of organic matter (Fig. 8a). The comparison results show that the proportion of aquatic organisms in organic matter composition of black shale is greater than that of dark-grey mudstone. The Pr/Ph (Pristane/Phytane) ratio of dark-grey mudstone ranges from 0.90 to 1.56 (Table 3), with an average of 1.15, indicating that it was mainly formed in a weak reduction to weak oxidation environment (Fig. 9a). The Pr/Ph ratio of black shale ranges from 0.48 to 1.00 (Table 3), with an average of 0.79, indicating that it was mainly formed in a reduction environment (Fig. 9a). The abundances of Pr and Ph are lower than their adjacent *n*-alkanes. The Pr/nC_{17} and Ph/nC_{18} values of the dark-grey mudstone range from 0.22 to 0.56 and 0.14 to 0.50 (Table 3), respectively, indicating that it was mainly deposited in a weak oxidation environment and the origin of organic matter was a mixture of terrestrial organic matter and aquatic organic matter (Fig. 9b). However, the Pr/nC_{17} and Ph/nC_{18} values of the black shale range from 0.11 to 0.45 and 0.13 to 0.55 (Table 3), respectively, indicating that it was mainly deposited in a weak reduction environment and the origin of organic matter was mainly composed of aquatic organic matter (Fig. 9b).

Consequently, the Pr/Ph ratio and the cross plot of Pr/nC_{17} and Ph/nC_{18} indicate that the dark-grey mudstone was mainly deposited in a weak reduction environment, and the black shale was mainly deposited in a reduction environment. The (nC_{15}+ nC_{17}+ nC_{19})/ (nC_{27}+ nC_{29}+ nC_{31}) ratio and the cross plot of Pr/nC_{17} and Ph/nC_{18} indicate that the organic matter of dark-grey mudstone was a mixture of terrestrial higher plants and aquatic organisms, while the organic matter of black shale was mainly originated from aquatic organisms. In addition, the (nC_{15}+

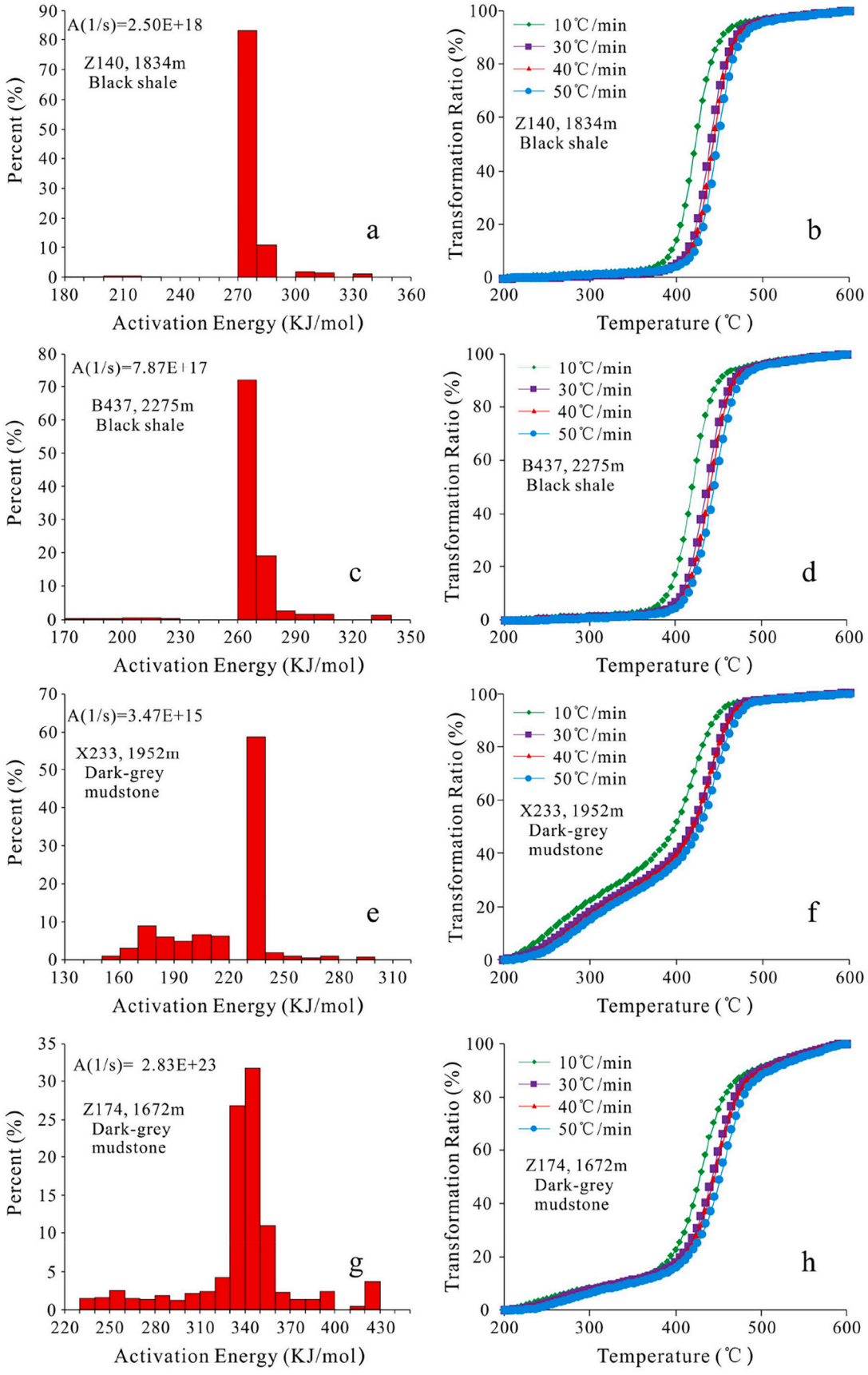

Fig. 4. Distribution characteristics of activation energy and hydrocarbon generation transformation rate of black shale and dark-grey mudstone in the Seventh Member of Yanchang Formation, Ordos Basin.

Table 1
Geochemical parameters, kinetics parameters and standard deviation of activation energy of dark-grey mudstone and black shale in the Seventh Member of Yanchang Formation, Ordos Basin.

Well/ Outcrop	Depth (m)	Lithology	TOC (%)	$S_1 + S_2$ (mg/g)	HI (mg/g)	Ro (%)	Kerogen type	Frequency Factor(S^{-1})	Weight average of activation energy (KJ/mol)	Standard deviation of activation energy (KJ/mol)
L42	2716	black shale	13.92	66.53	399	0.65	II_1	3.83E+10^{17}	225	20.91
B437	2275	black shale	33.17	130.36	381	0.73	II_1	7.87E+10^{17}	267	24.72
C98	2037	black shale	10.68	24.57	183	0.78	II_1	7.63E+10^{19}	292	28.93
Z140	1834	black shale	13.16	79.35	571	0.76	I	2.50E+10^{18}	274	23.73
TNH	/	black shale	39.30	191.49	421	0.59	II_1	2.77E+10^{17}	260	17.91
L32	2809	dark-grey mudstone	6.46	24.51	296	0.64	II_1	1.24E+10^{18}	285	24.27
C98	2040	dark-grey mudstone	1.98	4.85	209	0.73	II_2	3.22E+10^{14}	215	31.42
X233	1952	dark-grey mudstone	2.54	9.10	221	0.73	II_2	3.47E+10^{15}	219	25.21
B15	1944	dark-grey mudstone	2.06	3.16	180	0.79	II_2	6.17E+10^{15}	236	37.52
Z174	1672	dark-grey mudstone	7.35	3.75	163	0.76	II_2	2.83E+10^{23}	337	28.22

$nC_{17}+nC_{19})/(nC_{27}+nC_{29}+nC_{31})$ ratio of dark-grey mudstone and black shale is negatively correlated with the standard deviation of activation energy (Fig. 8b), indicating that the greater the relative proportion of terrestrial higher plants in organic matter, the more dispersed the distribution of activation energy. The low $(nC_{15}+nC_{17}+nC_{19})/(nC_{27}+nC_{29}+nC_{31})$ ratio of black shale outcrop sample (E-31) was mainly caused by weathering. Therefore, the relatively dispersed activation energy distribution of dark-grey mudstone is related to the large number of terrestrial organisms in its organic matter.

4.3.2.2. Terpanes. The C_{19-29} tricyclic terpanes (C_{19-29} TT), C_{24} tetracyclic terpane (C_{24} TeT) and pentacyclic terpanes (hopanes) are all detected in dark-grey mudstone and black shale of the Chang 7 Member (Fig. 7c and d). The abundances of C_{19-24} TT in black shale are higher than that in dark-grey mudstone (Fig. 7c and d). Higher abundance of tricyclic terpanes in black shale indicates that its organic matter contains higher algae (Volkman et al., 1989).

The abundance of C_{23}TT is higher and the $C_{21}TT/C_{23}TT$ ratio is 0.69–0.99 in dark-grey mudstone, while the abundance of C_{21}TT is higher and the $C_{21}TT/C_{23}TT$ ratio is 0.96–1.31 in black shale (Table 3). The $G/C_{30}H$ ratio of dark-grey mudstone ranges from 0.08 to 0.33, while the $G/C_{30}H$ ratio of black shale ranges from 0.01 to 0.10 (Table 4 and Fig. 10a). Generally, the source rocks deposited in saltwater lacustrine have the advantage of C_{23}TT and high $G/C_{30}H$ ratio, while the source rocks deposited in freshwater lacustrine have the advantage of C_{21}TT and low $G/C_{30}H$ ratio (Peters et al., 2005; Tao et al., 2015). Therefore, the higher abundance C_{23}TT and relatively high $G/C_{30}H$ ratio in dark-grey mudstone indicate that it is mainly deposited in brackish water environment. While the higher abundance C_{21}TT and low $G/C_{30}H$ ratio in black shale indicate that it is mainly deposited in freshwater environment (Peters et al., 2005; Tao et al., 2015). The $C_{24}TeT/(C_{24}TeT + C_{23}TT)$ ratios of dark-grey mudstone and black shale range from 0.26 to 0.42 and 0.17 to 0.27 (Table 3), respectively. The C_{24}TeT is believed to be originated from terrigenous organic matter (Philp and Gilbert, 1982). Therefore, the higher $C_{24}TeT/(C_{24}TeT + C_{23}TT)$ ratio of dark-grey mudstone samples indicates that the content of terrigenous organisms in dark-grey mudstone is higher than that of black shale (Philp and Gilbert, 1982; Connan et al., 1986; Peters et al., 2005). The C_{30} rearranged hopane (C_{30}RAH) is detected in dark-grey mudstone and black shale of the Chang 7 Member (Fig. 7c and d). But the abundance of C_{30}RAH is higher and the $C_{30}RAH/C_{30}H$ ratio ranges from 0.29 to 3.47 (average 0.99) in dark-grey mudstone, while the abundance of C_{30}RAH is lower and the $C_{30}RAH/C_{30}H$ ratio ranges from 0.07 to 0.54 (average 0.22) in black shale (Table 4). Higher $C_{30}RAH/C_{30}H$ ratio of dark-grey mudstone indicates that it is deposited in weak oxidation environment (Nytoft et al., 2006; Jin et al., 2019; Baydjanova and George, 2019). The ratios of C_{31} hopane 22S/(22S + 22R) of dark-grey mudstone and black shale range from 0.54 to 0.57 and 0.52 to 0.57(Table 4), respectively. The ratio of C_{31} hopane 22S/(22S + 22R) indicates that the maturity of dark-grey mudstone and black shale samples is close and ranging from low maturity to early stage of maturity, which is in agreement with the Ro data.

Consequently, the distribution characteristics of C_{21-23}TT, $G/C_{30}H$ and $C_{30}RAH/C_{30}H$ ratios indicate that the dark-grey mudstone is mainly deposited in the weak reduction brackish water environment, while the black shale is mainly deposited in the reduction freshwater environment. The $C_{24}TeT/(C_{24}TeT + C_{23}TT)$ ratio indicates that the proportion of terrestrial organisms in organic matter of dark-grey mudstone is greater than that of shale. In addition, the $C_{24}TeT/(C_{24}TeT + C_{23}TT)$ ratio of dark-grey mudstone and black shale is positively correlated with the standard deviation of activation energy (Fig. 8c) and weakly negatively correlated with the weighted average of activation energy (Fig. 8d), indicating that the dispersion degree of activation energy distribution of source rocks increases with the increase of terrestrial organic matter content, while the weighted average of activation energy decreases with the increase of terrestrial organic matter content. The results related to the complex maceral composition of terrestrial higher plants, and the activation energy distribution of different macerals is different (Sun et al., 1999; Jiang et al., 2005; Wang et al., 2017; Xu et al., 2018). Therefore, the activation energy distribution of dark-grey mudstone containing aquatic and terrestrial organisms is relatively dispersed, while the activation energy distribution of black shale dominated by aquatic organisms is relatively concentrated. In addition, the activation energy value of some macerals (eg. sporinite, cutinite and suberinite) from terrestrial higher plants is lower than that of alginite (Sun et al., 1999; Jiang et al., 2005; Wang et al., 2017; Xu et al., 2018), resulting in the decrease of weighted average activation energy of source rocks with the increase of terrestrial organic matter content.

4.3.2.3. Steranes. There are significantly differences in the abundance of short-chain steranes and regular steranes between dark-grey mudstone and black shale (Fig. 7e and f). The normalized distribution characteristics of C_{27-29} ααα*R* steranes of the Chang 7 Member source rocks show in Fig. 10b and Table 4. The dark-grey mudstone of the Chang 7 Member is characterized by a higher proportion of C_{29} ααα*R* sterane (26.11%- 58.48%), followed by C_{27} ααα*R* sterane (25.31%- 47.30%) and C_{28} ααα*R* sterane (15.68%- 33.15%) (Table 5). However, the black shale of the Chang 7 Member is characterized by a higher proportion of C_{27} ααα*R* sterane (26.47%- 52.70%), followed by C_{29} ααα*R* sterane (26.63%- 42.42%) and C_{28} ααα*R* sterane (20.32%- 35.91%)

Table 2
The geochemical parameters, organic maceral composition and maceral standard deviation of dark-grey mudstone and black shale in the Seventh Member of Yanchang Formation, Ordos Basin.

Sample Number	Well/ Outcrop	Deep (m)	Lithology	TOC (%)	$S_1 + S_2$ (mg/g)	HI (mg/g)	Tmax (°C)	Ro (%)	Relative percentages of maceral composition (%)			(Vitrinite +Inertinite)/Liptinite
									Liptinite	Vitrinite	Inertinite	
E-1	A84	2257	dark-grey mudstone	2.89	10.04	305	448	0.78	73.4	24.4	2.2	0.36
E-2	L32	2809	dark-grey mudstone	6.46	24.51	296	439	0.64	86.6	6.9	6.5	0.15
E-3	X59	2131	dark-grey mudstone	4.76	16.64	301	447	0.79	79.5	8.4	12.1	0.26
E-4	C75	2043	dark-grey mudstone	2.41	4.18	147	449	0.78	52.1	47.4	0.5	0.92
E-5	C75	2080	dark-grey mudstone	8.84	14.76	143	448	0.77	82.5	14.7	2.8	0.21
E-6	C75	2091	dark-grey mudstone	4.19	5.53	102	450	0.78	76.8	21.7	1.5	0.30
E-7	C75	2092	dark-grey mudstone	6.13	6.45	87	451	0.78	90.9	7.3	1.8	0.10
E-8	X233	1944	dark-grey mudstone	1.61	4.08	211	447	0.71	58.3	33.6	8.1	0.72
E-9	X233	1952	dark-grey mudstone	2.54	9.10	221	447	0.73	70.3	21.6	8.1	0.42
E-10	X233	1984	dark-grey mudstone	1.87	6.05	221	445	0.78	78.2	19.5	2.3	0.28
E-11	C98	2040	dark-grey mudstone	1.98	4.85	209	448	0.78	77.1	20.6	2.3	0.30
E-12	B15	1944	dark-grey mudstone	2.06	3.16	120	449	0.79	61.4	37.8	0.8	0.65
E-13	Z174	1673	dark-grey mudstone	7.35	3.75	142	446	0.76	71.1	24.8	4.1	0.41
E-14	Z80	2013	dark-grey mudstone	7.93	15.85	163	448	0.75	67.0	26.5	6.5	0.49
E-15	Zh98	2469	dark-grey mudstone	6.05	16.63	255	449	0.77	77.2	18.3	4.5	0.30
E-16	Zh98	2472	dark-grey mudstone	6.89	19.96	271	450	0.79	78.7	18.6	2.7	0.27
E-17	Zh98	2473	dark-grey mudstone	5.08	17.04	320	451	0.79	82.0	16.4	1.6	0.22
E-18	A84	2258	black shale	6.21	26.59	399	450	0.79	81.1	10.2	8.7	0.23
E-19	L42	2715	black shale	13.92	66.53	399	436	0.65	97.0	1.7	1.3	0.03
E-20	G252	2558	black shale	10.37	53.96	484	447	0.73	92.7	6.4	0.9	0.08
E-21	G252	2562	black shale	13.69	54.50	366	449	0.74	90.7	6.8	2.5	0.10
E-22	G252	2565	black shale	16.99	91.56	510	449	0.76	62.2	36.8	1.0	0.61
E-23	G252	2570	black shale	10.59	43.01	368	447	0.77	86.6	9.4	4.0	0.15
E-24	B437	2275	black shale	33.17	130.36	381	444	0.73	92.0	6.0	2.0	0.09
E-25	L79	2213	black shale	6.34	23.14	326	443	0.75	82.5	14.7	2.8	0.21
E-26	L79	2283	black shale	21.11	83.38	368	444	0.77	86.9	12.1	1.0	0.15
E-27	C98	2037	black shale	10.68	21.27	183	448	0.78	83.8	12.6	3.6	0.19
E-28	Z140	1834	black shale	13.16	76.74	571	447	0.76	84.0	11.5	4.5	0.20
E-29	TNH	/	black shale	35.59	150.38	405	430	0.59	92.0	6.0	2.0	0.09
E-30	TNH	/	black shale	39.39	174.30	424	432	0.61	93.0	4.0	3.0	0.08
E-31	TNH	/	black shale	39.30	178.79	422	430	0.59	90.3	7.6	2.1	0.11
E-32	HJF	/	black shale	32.84	135.09	383	433	0.62	92.4	7.2	0.4	0.08
E-33	HJF	/	black shale	27.83	87.47	295	438	0.64	82.5	14.9	2.6	0.21

(Table 5). The distribution characteristics of C_{27-29} ααα R steranes indicates that the organic matter of dark-grey mudstone and black shale mainly origins from algae, terrestrial higher plants and bacteria (Fig. 10b). The difference is that the proportion of terrestrial higher plants in the organic matter of dark-grey mudstone is higher than that of black shale. The composition of aquatic organisms is simple and the activation energy of different macerals are similar, while the composition of terrestrial higher plants is complex and the activation energy of different macerals is different (Sun et al., 1999; Jiang et al., 2005; Wang et al., 2017; Xu et al., 2018). Therefore, the activation energy of dark-grey mudstone containing aquatic and terrestrial organic matter is more dispersed than that of black shale.

The ratios of C_{29} ααα20S/(20S + 20R) steranes of dark-grey mudstone and black shale range from 0.38 to 0.51 and 0.35 to 0.49 (Table 4 and Fig. 3d), respectively. The ratios of C_{29} ββ/(ββ + αα) steranes of dark-grey mudstone and black shale range from 0.47 to 0.59 and 0.40 to 0.59 (Table 4 and Fig. 3d), respectively. The ratios of C_{29} ααα20S/(20S + 20R) and C_{29} ββ/(ββ + αα) steranes indicate that the maturity of dark-grey mudstone and black shale samples is close and in the early stage of maturity, which is basically consistent with the Ro data.

4.3.2.4. Aromatic hydrocarbons. The Fig. 7g and h representatively show the total ion chromatograms of the aromatic fraction selected from dark-grey mudstone (Fig. 7g) and black shale (Fig. 7h) in the Chang 7 Member. The aromatic fraction of dark-grey mudstone is characterized by low concentrations of methylnaphthalenes (MNs, $m/z = 142$) and dimethylnaphthalenes (DMNs, $m/z = 156$), and high concentrations of trimethylnaphthalenes (TMMs, $m/z = 170$) and dimethylphenanthrenes (DMPs, $m/z = 206$) (Fig. 7g). The aromatic fraction of black shale has the characteristics of relatively high concentrations of the MNs and DMNs, high concentrations of the TMNs and relatively low DMPs

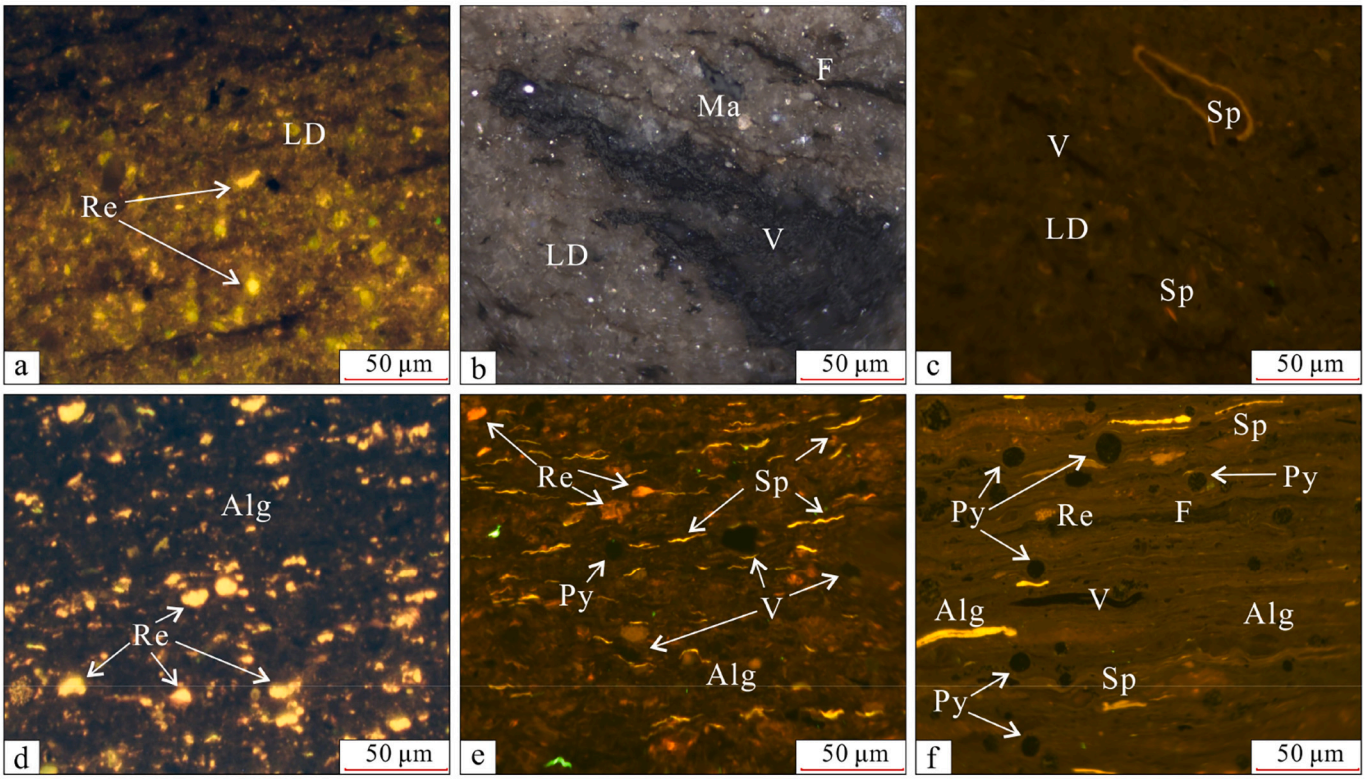

Fig. 5. Representative maceral photos of dark-grey mudstone (a-c) and black shale (d-f) in the Seventh Member of Yanchang Formation under the incident white light (b) and fluorescence mode (a, c, d, e, f). (a. L32, 2809 m, dark-grey mudstone; b. X233, 1952 m, dark-grey mudstone; c. C98, 2040 m, dark-grey mudstone; d. G252, 2558 m, black shale; e. B437, 2275 m, black shale; f. TNH, black shale. LD: liptodetrinite; V: vitrinite; Sp: sporinite; Alg: alginite; Ma: macrinite; F: fusinite; Re: resinite; Py: pyrite).

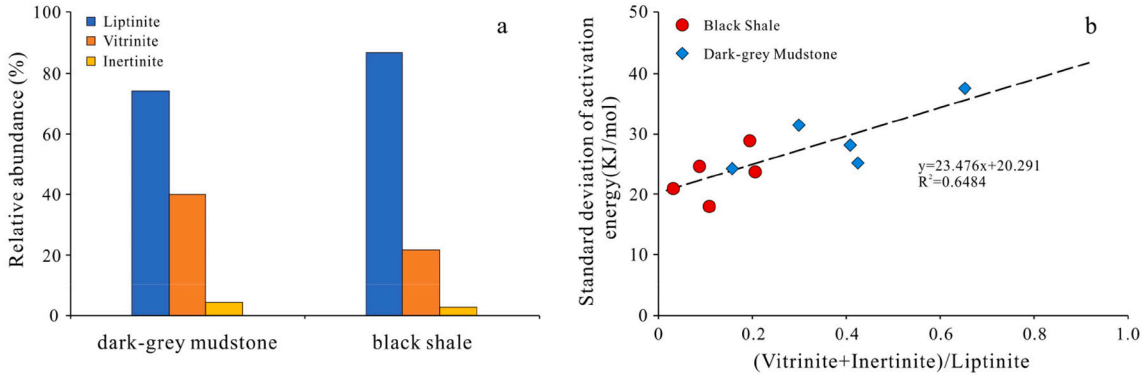

Fig. 6. Distribution characteristics of organic macerals between black shale and dark-grey mudstone (a), and correlation between the standard deviation of activation energy and the ratio of (Vitrinite+Inertinite)/Liptinite (b) in the Seventh Member of Yanchang Formation (Chang 7 Member), Ordos Basin.

(Fig. 7h). However, the distribution characteristics of the MNs, ethylnaphthalenes (ENs, m/z = 156), DMNs, TMNs and tetramethylnaphthalenes (TeMNs, m/z = 184) in dark-grey mudstone and black shale are similar (Fig. 7g and h). The predominant compounds of the ENs, DMNs, TMNs and TeMNs are 1-MN, 2-EN, 1,6-DMN, 1,3,6-TMN and 1,3,6,7-TeMN, respectively. Moreover, the distribution characteristics of methylphenanthrenes (MPs, m/z = 192) and the DMPs in dark-grey mudstone and black shale are also similar, and the contents of 9-MP and 1,3 − +3,9 − +3,10 − +2,10-DMP are the highest (Fig. 7g and h).

The MPI-1 values (Cassani et al., 1988) of dark-grey mudstone and black shale are 0.44–0.70 and 0.34–0.62, respectively, and the corresponding calculated reflectance values (Radke and Welte, 1983) are 0.66%–0.82% and 0.60%–079% (Table 5), respectively. The MDR values (Radke et al., 1986) of dark-grey mudstone and black shale are 1.86–4.05 and 1.30–3.69, respectively, and the corresponding calculated reflectance values (Kvalheim et al., 1987) are 0.65%–0.81% and 0.61%–078% (Table 5), respectively. The MPI-1 and MDR values also indicate a thermal maturity of dark-grey mudstone and black shale between low maturity and the early stage of maturity, which is basically consistent with the results of the Ro data, hopane and sterane isomerization parameters.

The normalized distribution characteristics of dibenzothiophene (DBT), dibenzofuran (DBF) and fluorene (F) show in Fig. 11a and Table 5. The relative concentration of DBT (30.86%- 73.64%) is the highest in dark-grey mudstone, followed by DBF (16.21%- 34.33%) and F (7.98%- 52.81%). The content of DBT (62.07%- 93.75%) in black shale is higher than that in dark-grey mudstone, while the contents of DBF (2.26%- 28.02%) and F (3.99%- 12.65%) are lower than that in dark-

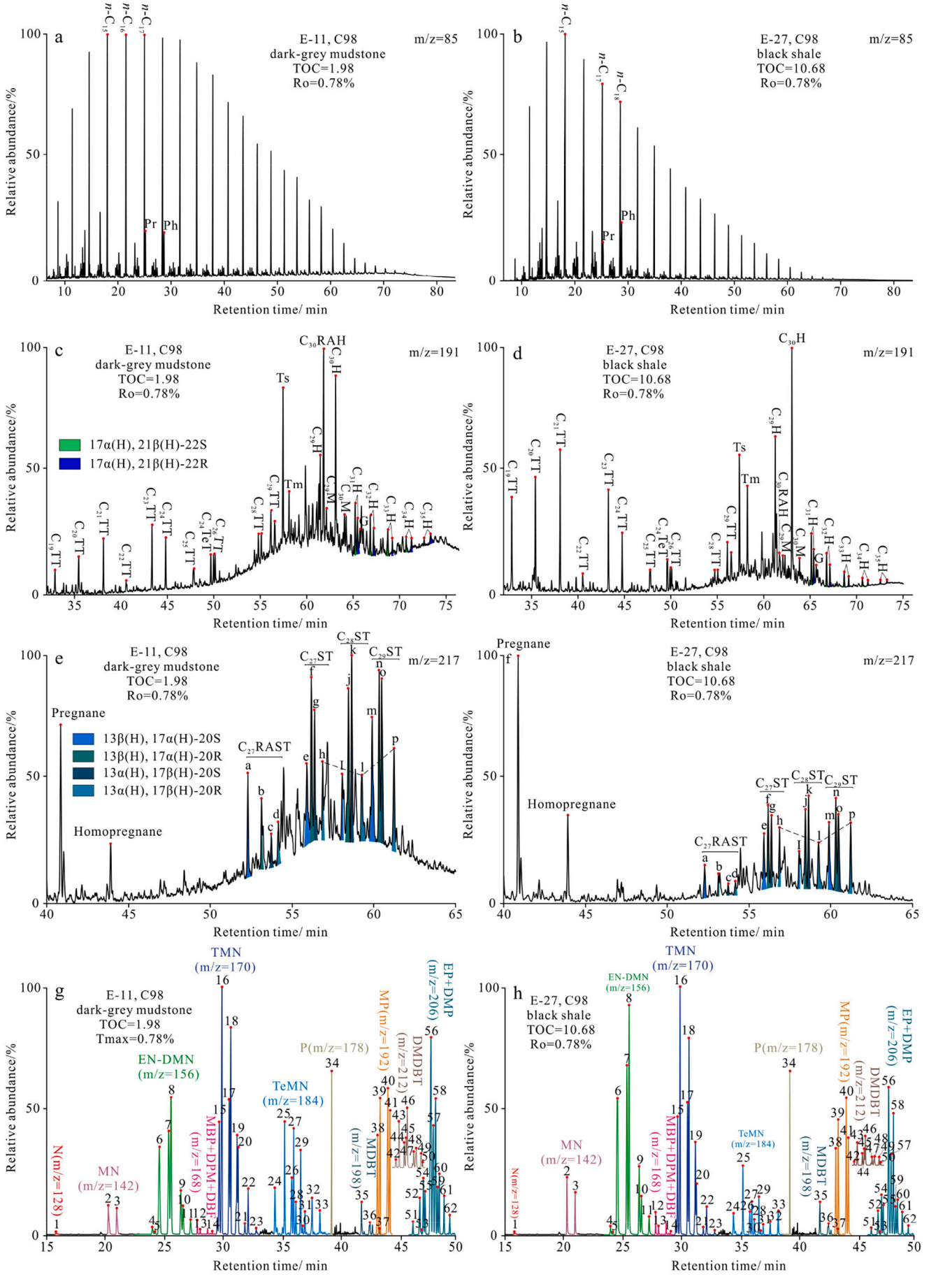

(caption on next page)

Fig. 7. Comparison of saturated and aromatic compounds between mudstone and shale in the Seventh Member of Yanchang Formation, Ordos Basin. a and b: m/z = 85 gas chromatographic mass spectrometry diagrams (*n*-alkanes); c and d: m/z = 191 gas chromatographic mass spectrometry diagrams (terpanes); e and f: m/z = 217 gas chromatographic mass spectrometry diagrams (steranes); g and h: total ion chromatogram (TIC) of aromatic hydrocarbon fractions. The details of the peak are given in the Appendix.

Table 3
Biomarker parameters of dark-grey mudstone and black shale in the Seventh Member of Yanchang Formation, Ordos Basin (TT: tricyclic terpanes, TeT: tetracyclic terpanes).

Sample Number	Lithology	$nC_{15+17+19}/nC_{27+29+31}$	Pr/Ph	Pr/nC_{17}	Ph/n-C_{18}	C_{21}/C_{23}TT	C_{24}TeT/(C_{24}TeT + C_{23}TT)
E-1	dark-grey mudstone	7.00	1.50	0.25	0.17	0.76	0.32
E-2	dark-grey mudstone	3.42	1.05	0.28	0.28	0.82	0.31
E-3	dark-grey mudstone	3.71	1.56	0.22	0.14	0.91	0.32
E-4	dark-grey mudstone	2.78	1.06	0.26	0.24	0.85	0.26
E-5	dark-grey mudstone	0.77	1.03	0.47	0.29	0.96	0.38
E-6	dark-grey mudstone	4.44	1.11	0.29	0.27	0.94	0.36
E-7	dark-grey mudstone	4.35	1.01	0.33	0.33	0.99	0.42
E-8	dark-grey mudstone	2.64	1.04	0.32	0.32	0.97	0.39
E-9	dark-grey mudstone	2.07	0.90	0.48	0.50	0.69	0.33
E-10	dark-grey mudstone	3.24	1.14	0.30	0.27	0.86	0.34
E-11	dark-grey mudstone	3.32	1.13	0.27	0.25	0.86	0.33
E-12	dark-grey mudstone	1.08	1.27	0.56	0.42	0.86	0.36
E-13	dark-grey mudstone	6.38	1.07	0.23	0.23	0.81	0.26
E-14	dark-grey mudstone	6.45	1.08	0.22	0.22	0.84	0.40
E-15	dark-grey mudstone	5.26	1.16	0.23	0.21	0.76	0.37
E-16	dark-grey mudstone	4.39	1.22	0.23	0.20	0.83	0.37
E-17	dark-grey mudstone	5.01	1.30	0.24	0.20	0.89	0.36
E-18	black shale	9.88	1.00	0.18	0.19	1.03	0.27
E-19	black shale	10.99	0.97	0.22	0.25	1.09	0.26
E-20	black shale	8.24	0.96	0.18	0.21	0.98	0.24
E-21	black shale	11.50	0.98	0.17	0.19	1.03	0.24
E-22	black shale	10.75	0.92	0.16	0.19	1.07	0.22
E-23	black shale	7.83	0.93	0.22	0.25	0.96	0.26
E-24	black shale	7.67	0.79	0.13	0.13	1.17	0.24
E-25	black shale	9.58	0.71	0.35	0.55	1.14	0.18
E-26	black shale	16.96	0.79	0.11	0.16	1.28	0.17
E-27	black shale	6.80	0.70	0.34	0.35	1.07	0.23
E-28	black shale	11.35	0.70	0.30	0.36	1.31	0.24
E-29	black shale	3.93	0.73	0.40	0.45	1.08	0.24
E-30	black shale	3.87	0.64	0.45	0.55	1.06	0.22
E-31	black shale	3.25	0.78	0.34	0.44	1.06	0.21
E-32	black shale	6.27	0.48	0.26	0.44	0.99	0.23
E-33	black shale	7.86	0.48	0.26	0.45	1.12	0.24

grey mudstone (Fig. 11a, Table 5). The abundance of DBT in dark-grey mudstone and black shale is high, indicating that its organic matter is deposited in reduction environment. The DBT/P ratios of dark-grey mudstone and black shale are 0.01–0.10 and 0.06–0.34 (Table 5), respectively. According to the cross plot of BDT/P vs. Pr/Ph proposed by Hughes et al. (1995), the dark-grey mudstone and black shale of the Chang 7 Member are deposited in the sulfate-poor lacustrine environment (Fig. 11b). Therefore, the dark-grey mudstone was mainly deposited in weak reduction environment, and the black shale was mainly deposited in reduction environment.

Some aromatic hydrocarbon compounds, such as the 1,2,5-TMN, 1,7-DMP and 1-MP, can be derived from conifers (Alexander et al., 1988). These compounds were detected in dark-grey mudstone and black shale of the Chang 7 Member, indicating that substantial terrestrial organic matter composed of conifers was inputted into the palo-lake during the deposition of the dark-grey mudstone and black shale. The palynoflora of the Chang 7 Member is dominated by *Paleoconiferus* and *Protoconiferus* (Ji and Meng, 2006), which also indicates that conifers are the primary terrestrial organic matter in the paleo-sedimentary environment. Retene is considered to origin from conifers, while the 1,3,6,7-TeMN is derived from bacteria (Püttmann and Villar, 1987; Peters et al., 2005; Romero-Sarmiento et al., 2011). Therefore, the retene/ 1,3,6,7-TeMN ratio can be used to describe the percentage of higher plants in organic matter. The retene/ (1,3,6,7- TeMN) ratio of dark-grey mudstone varies from 0.11 to 0.27, with an average of 0.17. Whereas, the retene/ (1,3,6,7- TeMN) ratio of black shale varies from 0.05 to 0.19, with an average of 0.11 (Table 5). The higher retene/ (1,3,6,7- TeMN) ratio of dark-grey mudstone indicates that the content of conifers in organic matter of dark-grey mudstone is higher than that of black shale. Moreover, the appearance of perylene in dark mudstone and black shale also indicates the existence of higher plants in organic matter (Fig. 12). The retene/ (1,3,6,7- TeMN) ratio of dark-grey mudstone and black shale is positively correlated with the standard deviation of activation energy (Fig. 8e), indicating that the dispersion degree of activation energy distribution of source rocks increases with the increase of conifers content. The relationship between retene/ (1,3,6,7- TeMN) ratio and the standard deviation of activation energy further proves that the input of terrestrial organic matter has an important influence on the activation energy distribution of source rocks. The greater the input of terrestrial organic matter, the more dispersed the activation energy of source rocks.

The polycyclic aromatic hydrocarbons (PAHs), such as pyrene, fluoranthene and chrysene, are usually associated with wildfire events (Jiang et al., 1998; Romero-Sarmiento et al., 2011). These compounds all detected in dark-grey mudstone and black shale, indicating wildfire events occurred around the deposition center. Previous studies have shown that the Qingling Mountain area experienced frequent volcanic activity during the deposition of the Chang 7 Member source rocks (Zhang et al., 2017; Zhang et al., 2020; Li et al., 2020), thus, the wildfire event was related to the volcanic activity. Affected by volcanic ash, hydrogen-rich algae were blooming and improved the primary productivity during the sedimentary period of black shale in the Chang 7 Member, which was supported by a large number of alginites in its macerals. In the meantime, the prosperity of bacteria and algae consumed oxygen and formed an anoxic paleo-environment, which was

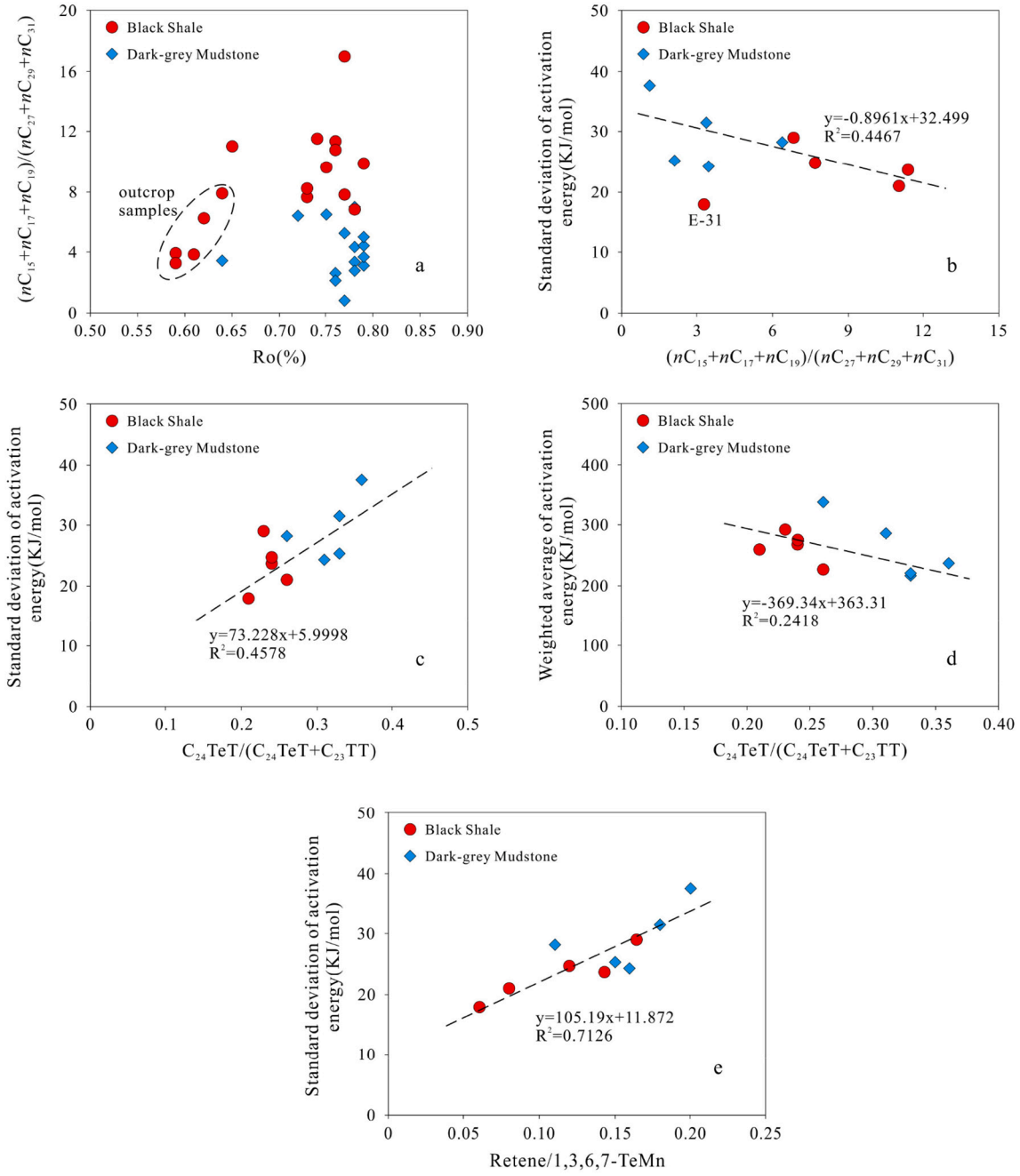

Fig. 8. Geochemical, activation energy and biomarker parameters intersection diagram of dark-grey mudstone and black shale in the Seventh Member of Yanchang Formation. (a) (*n*C15+ *n*C17+ *n*C19)/ (*n*C27+ *n*C29+ *n*C31) vs. Ro; (b) Standard deviation of activation energy vs. (*n*C15+ *n*C17+ *n*C19)/ (*n*C27+ *n*C29+ *n*C31); (c) Standard deviation of activation energy vs. C_{24}TeT/ (C_{24}TeT+ C_{23}TT); (d) Weight average of activation energy vs. C_{24}TeT/ (C_{24}TeT+ C_{23}TT); (e) Standard deviation of activation energy vs. Retene/1,3,6,7-TeMn.

supported by its low Pr/Ph ratio, high abundance of DBT. On the contrary, volcanic activity was weak during the sedimentary period of dark-grey mudstone in the Chang 7 Member, and the origin and sedimentary environment of organic matter were mainly controlled by terrestrial organic matter input, which was supported by a large amount of vitrinite in its macerals. Affected by the input of terrestrial organic matter, the sedimentary environment of dark-grey mudstone was a weak reduction environment, which was supported by its high Pr/Ph ratio, low abundance of DBT. Thus, high paleo-productivity and anoxic preservation condition make the abundance and kerogen type of organic matter in black shale are better than that in dark-grey mudstone, and the hydrocarbon generation potential of black shale is higher than that of dark mudstone.

4.3.3. *Influence of clay minerals and radioactive elements*

The mineralogical composition of dark-grey mudstone is composed of clay (43.4%), quartz (21.5%), k-feldspar (1.0%), plagioclase (7.1%), calcite (0.7%), dolomite (5.0%), pyrite (2.3%) and other amorphous minerals (19.0%), while the mineralogical composition of black shale is composed of clay (52.1%), quartz (12.5%), k-feldspar (1.9%), plagioclase (7.1%), calcite (0.3%), dolomite (5.5%), pyrite (7.6%) and other amorphous minerals (13.0%) (Lin et al., 2017; Liu et al., 2018). The quartz, feldspar, calcite and dolomite have no obvious effect on the hydrocarbon generation process of kerogen pyrolysis (Gao et al., 1990). The clay minerals as catalytic can reduce the activation energy of hydrocarbon generation reaction and accelerate the reaction rate (Johns and Shimoyama, 1972; Eglinton et al., 1986). Therefore, affected by the

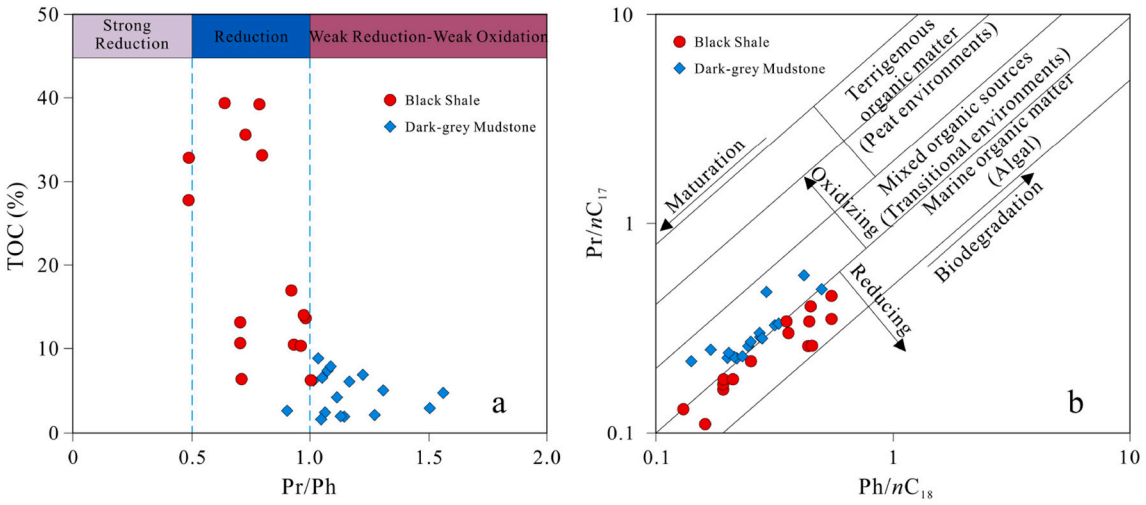

Fig. 9. Biomarker parameters intersection diagram of dark-grey mudstone and black shale in the Seventh Member of Yanchang Formation. (a) TOC vs. Pr/Ph; (b) Pr/nC_{17} vs. Ph/nC_{18}.

Table 4
Biomarker parameters of dark-grey mudstone and black shale in the Seventh Member of Yanchang Formation, Ordos Basin (G: gammacerane, H: hopane, RAH: rearranged hopane,).

Sample Number	Lithology	G/C_{30}H	C_{30}RAH/C_{30}H	C_{31} hopane S/(S + R)	$C_{29}\beta\beta/(\beta\beta+\alpha\alpha)$	$C_{29}\alpha\alpha\alpha$20S/(20S + 20R)	Normalized distribution of $C_{27-29}\alpha\alpha\alpha$R steranes (%)		
							C_{27}	C_{28}	C_{29}
E-1	dark-grey mudstone	0.16	0.58	0.56	0.55	0.40	28.25	20.27	51.47
E-2	dark-grey mudstone	0.13	0.63	0.54	0.47	0.38	25.31	18.16	56.53
E-3	dark-grey mudstone	0.17	0.98	0.56	0.57	0.50	39.53	19.51	40.96
E-4	dark-grey mudstone	0.24	1.86	0.55	0.51	0.45	40.95	20.47	38.57
E-5	dark-grey mudstone	0.16	0.90	0.57	0.54	0.46	28.31	15.68	56.01
E-6	dark-grey mudstone	0.12	0.53	0.56	0.52	0.45	29.70	33.15	37.15
E-7	dark-grey mudstone	0.13	0.50	0.59	0.57	0.50	28.86	29.02	42.12
E-8	dark-grey mudstone	0.11	0.59	0.55	0.54	0.48	41.86	23.21	34.93
E-9	dark-grey mudstone	0.09	0.31	0.56	0.51	0.47	38.33	26.81	34.86
E-10	dark-grey mudstone	0.16	1.19	0.57	0.54	0.46	47.30	18.94	33.76
E-11	dark-grey mudstone	0.20	1.27	0.56	0.54	0.47	46.43	27.46	26.11
E-12	dark-grey mudstone	0.23	3.47	0.57	0.56	0.49	25.48	16.04	58.48
E-13	dark-grey mudstone	0.33	2.12	0.54	0.52	0.44	45.14	22.65	32.21
E-14	dark-grey mudstone	0.12	0.82	0.55	0.54	0.50	30.82	27.76	41.42
E-15	dark-grey mudstone	0.09	0.29	0.56	0.56	0.45	25.83	27.96	46.21
E-16	dark-grey mudstone	0.09	0.37	0.57	0.60	0.49	29.48	27.49	43.03
E-17	dark-grey mudstone	0.08	0.38	0.57	0.59	0.51	28.08	28.16	43.76
E-18	black shale	0.08	0.51	0.57	0.55	0.49	52.70	20.32	26.97
E-19	black shale	0.04	0.21	0.52	0.47	0.42	48.30	25.08	26.63
E-20	black shale	0.02	0.11	0.54	0.45	0.41	43.42	23.72	32.87
E-21	black shale	0.03	0.11	0.55	0.44	0.41	43.62	23.28	33.10
E-22	black shale	0.01	0.16	0.56	0.56	0.49	46.38	24.96	28.66
E-23	black shale	0.01	0.15	0.57	0.58	0.46	47.33	23.12	29.55
E-24	black shale	0.06	0.29	0.54	0.53	0.46	30.63	33.45	35.92
E-25	black shale	0.06	0.48	0.56	0.54	0.47	45.60	25.49	28.91
E-26	black shale	0.03	0.30	0.57	0.57	0.47	41.10	29.27	29.63
E-27	black shale	0.06	0.54	0.57	0.59	0.48	38.08	30.86	31.06
E-28	black shale	0.10	0.27	0.55	0.54	0.49	29.32	35.91	34.77
E-29	black shale	0.07	0.07	0.52	0.41	0.35	31.41	31.85	36.74
E-30	black shale	0.07	0.07	0.53	0.42	0.36	26.47	31.11	42.42
E-31	black shale	0.07	0.07	0.53	0.43	0.36	27.65	31.50	40.85
E-32	black shale	0.07	0.07	0.53	0.40	0.35	29.09	29.77	41.14
E-33	black shale	0.07	0.07	0.54	0.41	0.36	29.01	29.57	41.42

influence of clay minerals, the hydrocarbon conversion rate of dark-grey mudstone and black shale increases after reaching the hydrocarbon generation threshold, and the hydrocarbon conversion rate of black shale containing more clay minerals is higher than that of dark-grey mudstone.

The black shale is more enriched in uranium (U) than dark-grey mudstone (Liu et al., 2018). The huge heat generated by the radioactive decay of uranium increases the thermal maturity of organic matter, which increases the hydrocarbon generation conversion rate of organic matter (Mao et al., 2012a, 2012b, 2014). Therefore, affected by the influence of uranium, the conversion rate of black shale is higher than that of dark-grey mudstone during the peak oil window.

In summary, the distribution of activation energy of dark-grey mudstone is dispersed, and its hydrocarbon generation process is characterized by low hydrocarbon generation threshold, slow conversion rate and long hydrocarbon generation cycle. The distribution of

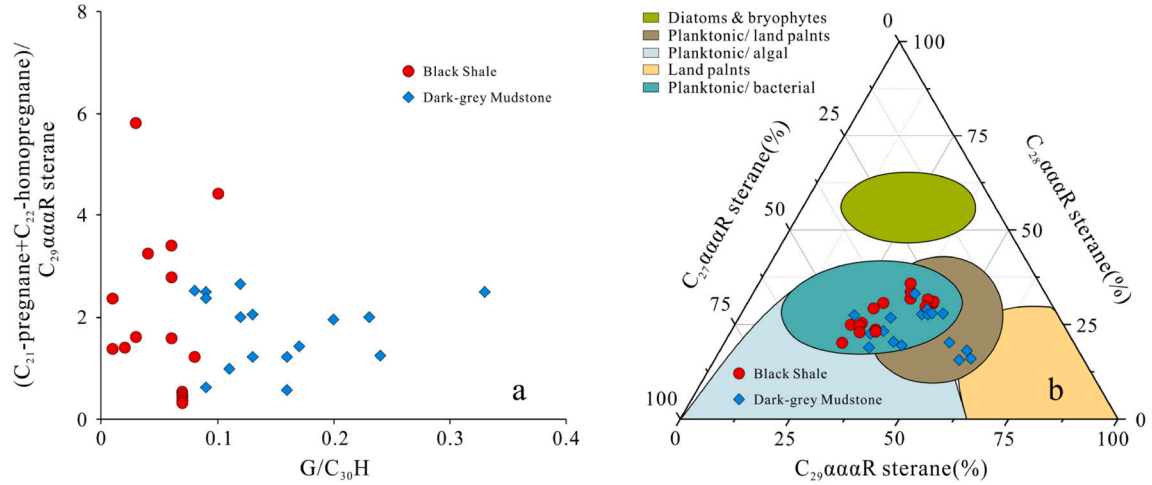

Fig. 10. Biomarker parameters intersection diagram of dark-grey mudstone and black shale in the Seventh Member of Yanchang Formation. (a) (C_{21}-pregnane+ C_{22}-homopregnane)/C_{29}ααα R sterane vs. G/C_{30}H; (b) ternary diagram of showing the proportions of C_{29}, C_{28} and C_{29}ααα R steranes (after Moldowan et al., 1985).

Table 5
Biomarker parameters of dark-grey mudstone and black shale in the Seventh Member of Yanchang Formation, Ordos Basin. (DBT: dibenzothiophene, DBF: dibenzofuran, F: fluorene, P: phenanthrene, TeMN: tetramethylnaphthalene).

Sample Number	Lithology	Normalized distribution of DBT, DBF and F (%)			DBF/P	Retene/1,3,6,7-TeMn	MPI-1	VR_{MPI} (%)	MDR	VR_{MDR} (%)
		DBT	DBF	F						
E-1	dark-grey mudstone	63.56	20.61	15.83	0.10	0.13	0.61	0.77	3.76	0.78
E-2	dark-grey mudstone	54.96	26.34	18.70	0.09	0.16	0.44	0.66	1.86	0.65
E-3	dark-grey mudstone	47.98	29.67	22.35	0.08	0.08	0.64	0.78	3.79	0.79
E-4	dark-grey mudstone	73.64	16.21	10.15	0.09	0.27	0.63	0.78	3.75	0.78
E-5	dark-grey mudstone	54.95	29.02	16.03	0.01	0.17	0.65	0.79	3.18	0.74
E-6	dark-grey mudstone	66.11	17.28	16.61	0.06	0.19	0.68	0.81	3.77	0.79
E-7	dark-grey mudstone	60.33	21.57	18.10	0.07	0.18	0.70	0.82	3.16	0.74
E-8	dark-grey mudstone	66.80	20.36	12.84	0.04	0.20	0.66	0.80	3.46	0.76
E-9	dark-grey mudstone	52.85	32.62	14.53	0.07	0.15	0.64	0.78	3.56	0.77
E-10	dark-grey mudstone	40.59	33.48	25.93	0.04	0.12	0.69	0.81	3.63	0.77
E-11	dark-grey mudstone	61.68	23.89	14.43	0.06	0.18	0.65	0.79	3.56	0.77
E-12	dark-grey mudstone	56.08	22.93	20.99	0.07	0.20	0.62	0.77	4.05	0.81
E-13	dark-grey mudstone	30.86	16.33	52.81	0.04	0.11	0.63	0.78	3.07	0.73
E-14	dark-grey mudstone	49.45	31.28	19.27	0.03	0.16	0.65	0.79	3.33	0.75
E-15	dark-grey mudstone	56.24	34.33	9.44	0.09	0.12	0.61	0.77	3.23	0.75
E-16	dark-grey mudstone	62.49	28.85	8.65	0.09	0.13	0.62	0.77	3.58	0.77
E-17	dark-grey mudstone	65.54	26.48	7.98	0.09	0.14	0.64	0.78	3.67	0.78
E-18	black shale	71.98	20.11	7.91	0.09	0.11	0.65	0.79	3.69	0.78
E-19	black shale	68.89	23.88	7.23	0.06	0.08	0.43	0.66	1.96	0.65
E-20	black shale	73.31	17.34	9.35	0.07	0.07	0.53	0.72	3.12	0.74
E-21	black shale	86.18	4.69	9.13	0.08	0.19	0.59	0.75	3.37	0.76
E-22	black shale	77.63	13.26	9.11	0.10	0.13	0.61	0.77	3.56	0.77
E-23	black shale	89.11	3.16	7.73	0.09	0.15	0.60	0.76	3.10	0.74
E-24	black shale	93.75	2.26	3.99	0.07	0.12	0.53	0.72	3.46	0.76
E-25	black shale	81.44	7.98	10.58	0.12	0.06	0.59	0.75	3.07	0.73
E-26	black shale	79.56	10.31	10.13	0.11	0.06	0.65	0.79	3.09	0.74
E-27	black shale	81.68	15.30	3.02	0.08	0.17	0.64	0.78	3.44	0.76
E-28	black shale	70.34	19.61	10.04	0.09	0.14	0.63	0.78	3.36	0.76
E-29	black shale	92.41	2.91	4.67	0.33	0.09	0.39	0.63	1.39	0.61
E-30	black shale	80.34	12.82	6.83	0.34	0.06	0.34	0.60	1.30	0.60
E-31	black shale	86.87	5.31	7.81	0.31	0.06	0.33	0.60	1.45	0.62
E-32	black shale	62.10	28.02	9.88	0.31	0.06	0.35	0.61	1.52	0.62
E-33	black shale	62.07	25.29	12.65	0.21	0.05	0.37	0.62	1.58	0.63

MPI-1: methylphenanthrene index (1.89 × [3-MP + 2-MP]/ [P + 1.26 × (9-MP + 1-MP)]). Cassani et al., 1988.
VR_{MPI}: calculated reflectance from MPI-1 (0.60 × MPI-1 + 0.40). Radke and Welte, 1983.
MDR: methyldibenzothiophene ratio (4-MDBT/1-MDBT). Radke et al., 1986.
VR_{MDR}: calculated reflectance from MDR (0.073 × MDR + 0.51). Kvalheim et al., 1987

activation energy of black shale is concentrated, and its hydrocarbon generation process has the characteristics of relatively high hydrocarbon generation threshold, fast conversion rate and short hydrocarbon generation cycle. As discussed above, the dispersion degree of activation energy distribution of source rocks increases with the increase of vitrinite and inertinite content in macerals (Fig, 6b). The dispersion degree of activation energy distribution of source rocks increases with the increase of terrestrial organic matter content (Fig. 8b, c, e), while the weighted average of activation energy tends to decrease with the increase of terrestrial organic matter content (Fig. 8d). These correlations show that the distribution characteristics of activation energy of source rocks are affected by the composition of macerals and organic matter

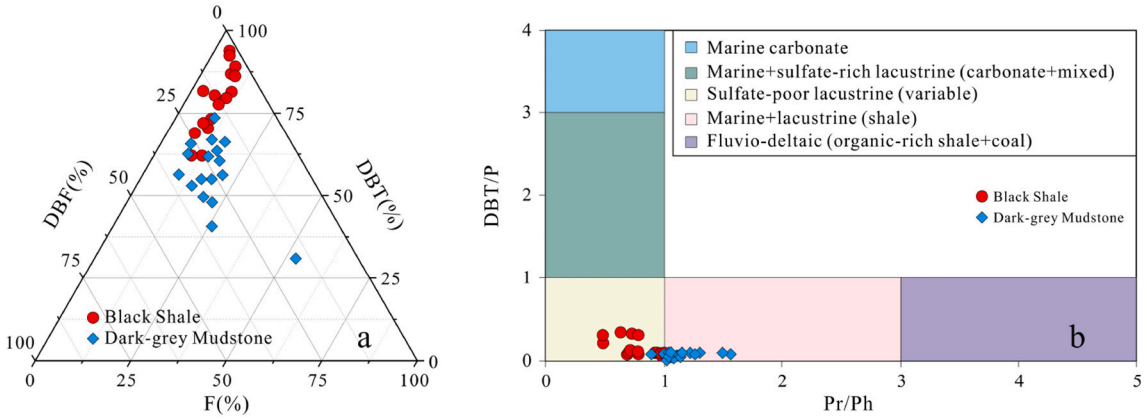

Fig. 11. Ternary diagram showing the proportions of dibenzothiophene (DBT), dibenzofuran (DBF) and fluorene (F) of dark-grey mudstone and black shale in the Seventh Member of Yanchang Formation (a); dibenzothiophene/ phenanthrene (BDT/P) ratio vs. Pr/Ph reflects source rock depositional environment (b) (after Hughes et al., 1995).

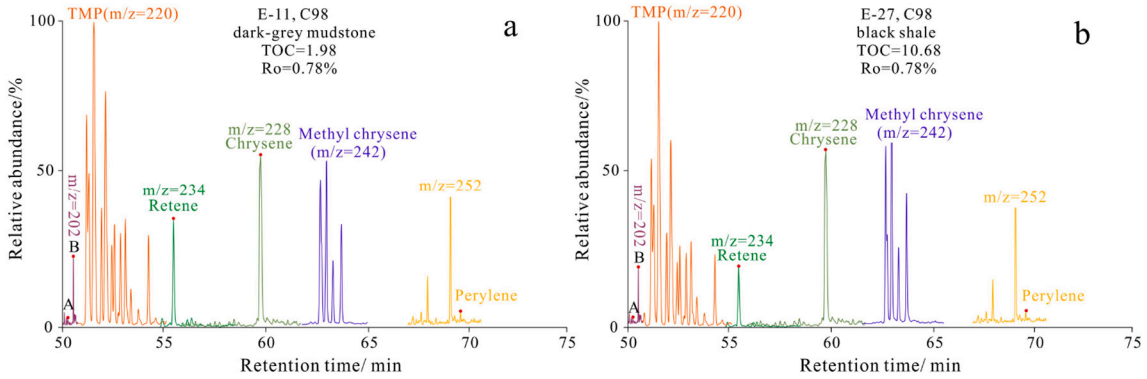

Fig. 12. Total ion chromatogram (m/z = 202, 220, 234, 228, 242, 252) of aromatic fractions of dark-grey mudstone and black shale in the Seventh Member of Yanchang Formation, Ordos Basin (A: fluoranthene; B: pyrene).

sources. The analysis results of biomarkers show that the organic matter of dark-grey mudstone mainly originates from algae and terrestrial higher plants (conifers), and the dark-grey mudstone was mainly deposited in weak oxidation to weak reduction environment. The organic matter of black shale mainly originates from algae, and the black shale was mainly deposited in reduction environment. The oxygenated conditions make the algae in organic matter of dark-grey mudstone easy to be biodegraded, and the macerals of dark-grey mudstone were mainly composed of vitrinite, liptodetrinite and inertinite. However, the anoxic conditions make the algae in organic matter of black shale can be well preserved, and the macerals of black shale were mainly composed of alginite. Therefore, the dispersion degree of activation energy of dark-grey mudstone containing a large number of terrestrial higher plants in organic matter is greater than that of black shale. The dispersed activation energy distribution of dark-grey mudstone results in its long hydrocarbon generation cycle and slow conversion rate after reaching the hydrocarbon generation threshold. The concentrated activation energy distribution of black shale results in its short hydrocarbon generation cycle and fast conversion rate after reaching the hydrocarbon generation threshold. In addition, affected by the macerals with lower activation energy, such as sporinite and resinite, the hydrocarbon generation threshold of dark-grey mudstone rich in terrestrial organic matter is lower than that of black shale. Moreover, radioactive elements (U) and more clay minerals in black shale also make its conversion rate higher than that of dark-grey mudstone.

5. Conclusions

(1) These evaluation parameters, such as TOC, $S_1 + S_2$ and HI, indicating that the dark-grey mudstone in the Chang 7 Member was classified as poor - very good source rocks, while the black shale was classified as very good - excellent source rocks. The activation energy distribution of dark-grey mudstone is dispersed, and its hydrocarbon generation process is characterized by low hydrocarbon generation threshold, slow transformation rate and long hydrocarbon generation cycle. While the activation energy distribution of black shale is concentrated, and its hydrocarbon generation process has the characteristics of relatively high hydrocarbon generation threshold, fast transformation rate and short hydrocarbon generation cycle.

(2) The dispersion degree of activation energy distribution of source rocks increases with the increase of vitrinite and inertinite content in macerals. The dispersion degree of activation energy distribution of source rocks increases with the increase of terrestrial organic matter content, while the weighted average of activation energy tends to decrease with the increase of terrestrial organic matter content. These correlations show that the distribution characteristics of activation energy of source rocks are affected by the composition of macerals and organic matter sources.

(3) The organic matter of dark-grey mudstone mainly originates from algae and terrestrial higher plants (conifers), while the organic matter of black shale mainly originates from algae. Under the influence of sedimentary environment, the macerals of dark-grey mudstone are mainly composed of vitrinite, liptodetrinite and

inertinite, while the macerals of black shale are mainly composed of alginite. The complex macerals composition and organic matter source make the activation energy distribution of dark-grey mudstone more dispersed than that of black shale. The dispersed activation energy distribution of dark-grey mudstone corresponds to long hydrocarbon generation cycle and slow conversion rate. The relative concentrated activation energy distribution of black shale corresponds to short hydrocarbon generation cycle and fast conversion rate. Affected by the macerals (such as sporinite and resinite) with lower activation energy, the hydrocarbon generation threshold of dark-grey mudstone is lower than that of black shale.

(4) The difference of mineral and element composition also affects the process and characteristics of hydrocarbon generation. The radioactive element (U) and more clay minerals in black shale make its conversion rate is higher than that of dark-grey mudstone during the peak oil window.

CRediT authorship contribution statement

Ruihui Zheng: Conceptualization, Writing – original draft, Resources. **Yifan Wang:** Supervision, Writing – review & editing. **Zhipeng Li:** Validation, Resources, Investigation. **Zhihuan Zhang:** Supervision, Funding acquisition. **Guangli Wang:** Investigation, Resources. **Heng Zhang:** Investigation.

Declaration of Competing Interest

The authors declare that they have no known competing financial interests or personal relationships that could have appeared to influence the work reported in this paper.

Acknowledgements

The corresponding author of this study was granted financial support by the China National Petroleum Corporation-China University of Petroleum (Beijing) Cooperation Science and Technology Project (Grant No. ZLZX2020-02-01-01). We sincerely thank two anonymous reviewers for their detailed and constructive comments that significantly improved the manuscript. In addition, Ruihui Zheng, the first author of the study, expressed his gratitude to Lile Tian for illuminating his present and future. Miss Lile Tian, will you marry him?

Appendix A

Table A.1
Identification of steranes and aromatic compounds in Fig. 6.

Compound group	Peak	Abbreviation	Biomarker	*m/z*
Steranes	a	$C_{27}\beta\alpha$ dia20S	20S-13β(H), 17α(H)-diacholestane	217
	b	$C_{27}\beta\alpha$ dia20R	20R-13β(H), 17α(H)-diacholestane	
	c	$C_{27}\alpha\beta$ dia20S	20S-13α(H), 17β(H)-diacholestane	
	d	$C_{27}\alpha\beta$ dia20R	20R-13α(H), 17β(H)-diacholestane	
	e	$C_{27}\alpha\alpha\alpha$ 20S	20S-5α(H), 14α(H), 17α(H)-cholestane	
	f	$C_{27}\alpha\beta\beta$ 20R	20R-5α(H), 14β(H), 17β(H)-cholestane	
	g	$C_{27}\alpha\beta\beta$ 20S	20S-5α(H), 14β(H), 17β(H)-cholestane	
	h	$C_{27}\alpha\alpha\alpha$ 20R	20R-5α(H), 14α(H), 17α(H)-cholestane	
	i	$C_{28}\alpha\alpha\alpha$ 20S	20S-24-Methyl-5α(H), 14α(H), 17α(H)-cholestane	
	j	$C_{28}\alpha\beta\beta$ 20R	20R-24-Methyl-5α(H), 14β(H), 17β(H)-cholestane	
	k	$C_{28}\alpha\beta\beta$ 20S	20S-24-Methyl-5α(H), 14β(H), 17β(H)-cholestane	
	l	$C_{28}\alpha\alpha\alpha$ 20R	20R-24-Methyl-5α(H), 14α(H), 17α(H)-cholestane	
	m	$C_{29}\alpha\alpha\alpha$ 20S	20S-24-Ethyl-5α(H), 14α(H), 17α(H)-cholestane	
	n	$C_{29}\alpha\beta\beta$ 20R	20R-24-Ethyl-5α(H), 14β(H), 17β(H)-cholestane	
	o	$C_{29}\alpha\beta\beta$ 20S	20S-24-Ethyl-5α(H), 14β(H), 17β(H)-cholestane	
	p	$C_{29}\alpha\alpha\alpha$ 20R	20R-24-Ethyl-5α(H), 14α(H), 17α(H)-cholestane	
Aromatic hydrocarbons	1	N	naphthalene	128
	2	2-MN	2-methylnaphthalene	142
	3	1-MN	1-methylnaphthalene	
	4	2-EN	2-ethylnaphthalene	156
	5	1-EN	1-ethylnaphthalene	
	6	2,6 − +2,7-DMN	2,6 − +2,7-dimethylnaphthalene	
	7	1,3 − +1,7-DMN	1,3 − +1,7-dimethylnaphthalene	
	8	1,6-DMN	1,6-dimethylnaphthalene	
	9	1,4 − +2,3-DMN	1,4 − +2,3-dimethylnaphthalene	
	10	1,5-DMN	1,5-dimethylnaphthalene	
	11	1,2-DMN	1,2-dimethylnaphthalene	
	12	3-MBP	3-methylbiphenyl	168
	13	4-MBP	4-methylbiphenyl	
	14	DBF	dibenzofuran	
	15	1,3,7-TMN	1,3,7-trimethylnaphthalene	170
	16	1,3,6-TMN	1,3,6-trimethylnaphthalene	
	17	1,4,6 − +1,3,5-TMN	1,4,6 − +1,3,5-trimethylnaphthalene	
	18	2,3,6-TMN	2,3,6-trimethylnaphthalene	
	19	1,2,7 − +167-TMN	1,2,7 − +167-trimethylnaphthalene	
	20	1,2,6-TMN	1,2,6-trimethylnaphthalene	
	21	1,2,4-TMN	1,2,4-trimethylnaphthalene	
	22	1,2,5-TMN	1,2,5-trimethylnaphthalene	
	23	1,4,5-TMN	1,4,5-trimethylnaphthalene	
	24	1,3,5,7-TeMN	1,3,5,7-tetramethylnaphthalene	184
	25	1,3,6,7-TeMN	1,3,6,7-tetramethylnaphthalene	
	26	1,4,6,7 − +1,2,4,6 − +1,2,4,7-TeMN	1,4,6,7 − +1,2,4,6 − +1,2,4,7-tetramethylnaphthalene	
	27	1,2,5,7 − +1,3,6,8-TeMN	1,2,5,7 − +1,3,6,8-tetramethylnaphthalene	
	28	2,3,6,7-TeMN	2,3,6,7-tetramethylnaphthalene	

(*continued on next page*)

Table A.1 (*continued*)

Compound group	Peak	Abbreviation	Biomarker	*m/z*
	29	1,2,6,7-TeMN	1,2,6,7-tetramethylnaphthalene	
	30	1,2,3,7-TeMN	1,2,3,7-tetramethylnaphthalene	
	31	1,2,3,6-TeMN	1,2,3,6-tetramethylnaphthalene	
	32	1,2,5,6 − +1,2,3,5 -TeMN	1,2,5,6 − +1,2,3,5 -tetramethylnaphthalene	
	33	DBT	dibenzothiophene	
	34	P	phenanthrene	178
	35	4-MDBT	4-methyldibenzothiophene	198
	36	2 − +3-MDBT	2 − +3-methyldibenzothiophene	
	37	1-MDBT	1-methyldibenzothiophene	
	38	3-MP	3-methylphenanthrene	192
	39	2-MP	2-methylphenanthrene	
	40	9-MP	9-methylphenanthrene	
	41	1-MP	1-methylphenanthrene	
	42	4-EDBT	4-ethyldibenzothiophene	212
	43	4,6-DMDBT	4,6-dimethyldibenzothiophene	
	44	2,4-DMDBT	2,4-dimethyldibenzothiophene	
	45	2,6-DMDBT	2,6-dimethyldibenzothiophene	
	46	3,6-DMDBT	3,6-dimethyldibenzothiophene	
	47	3,7-DMDBT	3,7-dimethyldibenzothiophene	
	48	1,4 − +1,6 + 1,8-DMDBT	1,4 − +1,6 + 1,8-dimethyldibenzothiophene	
	49	1,3 − +3,4-DMDBT	1,3 − +3,4-dimethyldibenzothiophene	
	50	1,2 − +1,9-DMDBT	1,2 − +1,9-dimethyldibenzothiophene	
	51	EP	ethylphenanthrene	206
	52	2-EP + 9-EP+ 3,6-DMP	2-ethylphenanthrene+9-ethylphenanthrene+3,6-dimethylphenanthrene	
	53	1-EP	1-ethylphenanthrene	
	54	2,6 − +2,7 − +3,5-DMP	2,6 − +2,7 − +3,5-dimethylphenanthrene	
	55	2,10- + 1,3- + 3,10- + 3,9-DMP	2,10- + 1,3- + 3,10- + 3,9-dimethylphenanthrene	
	56	1,6 − + 2,9- + 2,5-DMP	1,6 − + 2,9- + 2,5-dimethylphenanthrene	
	57	1,7-DMP	1,7-dimethylphenanthrene	
	58	2,3-DMP	2,3-dimethylphenanthrene	
	59	4,9- + 4,10- + 1,9-DMP	4,9- + 4,10- + 1,9-dimethylphenanthrene	
	60	1,8-DMP	1,8-dimethylphenanthrene	
	61	1,2-DMP	1,2-dimethylphenanthrene	

References

Alexander, R., Larcher, A.V., Kagi, R.I., Price, P.L., 1988. The use of plant derived biomarkers for correlation of oils with source rocks in the Cooper/Eromanga Basin System. Australia. Appea Journal 28 (1), 310–324.

Algeo, T.J., Kuwahara, K., Sano, H., Bates, S., Lyons, T., Elswick, E., Hinnov, L., Ellwood, B., Moser, J., Maynard, J.B., 2011. Spatial variation in sediment fluxes, redox conditions, and productivity in the Permian–Triassic Panthalassic Ocean. Palaeogeogr. Palaeoclimatol. Palaeoecol. 308 (1–2), 65–83.

Arthur, M.A., Dean, W.E., 1998. Organic-matter production and preservation and evolution of anoxia in the Holocene Black Sea. Paleoceanography 13 (4), 395–411.

Baydjanova, S., George, S.C., 2019. Depositional environment, organic matter sources, and variable 17α(H)-diahopane distribution in early Permian samples, southern Sydney Basin, Australia. Org. Geochem. 131, 60–75.

Cassani, F., Gallango, O., Talukdar, S., Vallejos, C., Ehrmann, U., 1988. Methylphenanthrene maturity index of marine source rock extracts and crude oils from the Maracaibo Basin. Org. Geochem. 13, 73–80.

Chen, Z.H., Guo, Q.L., Jiang, C.Q., Liu, X.J., Reyes, J., Mort, A., Jia, Z.K., 2017. Source rock characteristics and Rock-Eval-based hydrocarbon generation kinetic models of the lacustrine Chang-7 Shale of Triassic Yanchang Formation, Ordos Basin. China. International Journal of Coal Geology 182, 52–65.

Chen, J.Q., Pang, X.Q., Pang, H., Chen, Z.H., Jiang, C.Q., 2018. Hydrocarbon evaporative loss evaluation of lacustrine shale oil based on mass balance method: Permian Lucaogou Formation in Jimusaer Depression, Junggar Basin. Mar. Pet. Geol. 91, 422–431.

Chen, Y.H., Wang, Y.B., Guo, M.Q., Wu, H.Y., Li, J., Wu, W.T., Zhao, J.Z., 2020. Differential enrichment mechanism of organic matters in the marine-continental transitional shale in northeastern Ordos Basin, China: Control of sedimentary environments. Journal of Natural Gas Science and Engineering 83, 103625.

Chen, L., Jiang, S., Chen, P., Chen, X.H., Zhang, B.M., Zhang, G.T., Lin, W.B., Lu, Y.C., 2021a. Relative Sea-level changes and organic matter enrichment in the Upper Ordovician-lower Silurian Wufeng-Longmaxi Formations in the Central Yangtze area. China. Marine and Petroleum Geology 124, 104809.

Chen, L., Zhang, B.M., Jiang, S., Chen, X.H., Zhang, G.T., Chen, P., Lin, W.B., Liu, Z.H., 2021b. Geochemical characteristics of the Upper Devonian Shetianqiao Formation in the Shaoyang sag of Xiangzhong depression from Middle Yangtze area, South China: Implications for the depositional environment and organic matter enrichment. Palaeogeogr. Palaeoclimatol. Palaeoecol. 574, 110448.

Connan, J., Bouroullec, J., Dessort, D., Albrecht, P., 1986. The microbial input in carbonate-anhydrite facies of a sabkha palaeoenvironment from Guatemala: a molecular approach. Org. Geochem. 10, 29–50.

Demaison, G.J., Moore, G.T., 1980. Anoxic environments and oil source bed genesis. AAPG Bull. 64 (8), 1179–1209.

Dieckmann, V., Ondrak, R., Cramer, B., Horsfield, B., 2006. Deep basin gas: New insights from kinetic modelling and isotopic fractionation in deep-formed gas precursors. Mar. Pet. Geol. 23 (2), 183–199.

Eglinton, T.I., Rowland, S.J., Curtis, C.D., Douglas, A.G., 1986. Kerogen-mineral reactions at raised temperatures in the presence of water. Org. Geochem. 10 (4–6), 1041–1052.

Fan, B.J., Mei, Q.L., Wang, X.J., Meng, Y., Huang, Q.J., 2020. Geochemical comparison of mudstone and shale – a case study of the 7th member of Yanchang Formation in Ansai area. Ordos Basin. Oil & Gas Geology 41 (6), 1119–1128 (In Chinese with English abstract).

Fu, J.H., Li, S.X., Niu, X.B., Deng, X.Q., Zhou, X.P., 2020a. Geological characteristics and exploration of shale oil in Chang 7 Member of Triassic Yanchang Formation, Ordos Basin, NW China. Petroleum Exploration and Development 47 (5), 931–945.

Fu, S.T., Fu, J.H., Niu, X.B., Li, S.X., Wu, Z.Y., Zhou, X.P., Liu, J.Y., 2020b. Reservoir formation conditions and key technologies for explorationand development in Qingcheng large oilfield. Petroleum Research 5, 181–201.

Fu, S.T., Jin, Z.Y., Fu, J.H., Li, S.X., Yang, W.W., 2021. Transformation of understanding from tight oil to shale oil in the Member 7 of Yanchang Formation in Ordos Basin and its significance of exploration and development. Acta Pet. Sin. 42 (5), 561–569 (In Chinese with English abstract).

Gao, X.Z., Zhang, W.X., Zhang, H.F., 1990. Study of influence of minerals on pyrolysis. Pet. Geol. Exp. 12 (2), 201–205 (In Chinese with English abstract).

Gelpi, E., Schneider, H., Mann, J., Oró, J., 1970. Hydrocarbons of geochemical significance in microscopic alage. Phytochemistry 9 (3), 603–612.

George, S.C., Ruble, T.E., Dutkiewicz, A., Eadington, P.J., 2001. Assessing the maturity of oil trapped in fluid inclusions using molecular geochemistry data and visually-determined fluorescence colours. Appl. Geochem. 16 (4), 451–473.

Hou, L.H., Lin, S.H., Zhang, L.J., 2021. New insights from geostatistics on the genetic relationship between shales, mudstones, and sandstones within a parasequence in the lower Chang7 Member of the Upper Triassic Yanchang Formation, Ordos Basin, Northern China. Journal of Asian Earth Science 213, 104767.

Hu, S.Z., Song, Y., Su, P., Mahlstedt, N., Mangelsdorf, K., Shen, C.B., Li, S.F., Zhu, K., 2020. Impact of marine incursions on lacustrine source rocks: organic matter quantity, quality, and kinetics in the Paleocene South Yellow Sea Basin, offshore eastern China. Org. Geochem. 148, 104084.

Huang, C.X., Zhang, Z.H., Li, X.Y., Deng, N.T., Yan, H.X., Bai, X., Luo, M.J., 2013. Hydrocarbon generation kinetics and simulation result analysis of source rocks in Yanchang Formation of the Southern Ordos Basin. Journal of Oil and Gas Technology 35 (8), 21–27 (In Chinese with English abstract).

Hughes, W.B., Holba, A.G., Dzou, L.J.P., 1995. The ratios of dibenzothiophene to phenanthrene and pristane to phytane as indicators of depositional environment and

lithology of petroleum source rocks. Geochim. Cosmochim. Acta 59 (17), 3581–3598.
ICCP, 1998. The new vitrinite classification (ICCP System 1994). Fuel 77, 349–358.
ICCP, 2001. The new vitrinite classification (ICCP System 1994). Fuel 80, 459–471.
ISO 7404-2, 2009. Methods for the petrographic analysis of coals- part 2: Methods of preparing coal samples. In: International Organization for Standardization. ISO 7404–2. https://www.iso.org/standard/42798.html.
Ji, L.M., Meng, F.W., 2006. Palynology of Yanchang Formation of Middle and late Triassic in Eastern Gansu Province and its Paleoclimatic significance. J. China Univ. Geosci. 17 (3), 209–220.
Jiang, C.Q., Alexander, R., Kagi, R., Murray, A.P., 1998. Polycyclic aromatic hydrocarbons in ancient sediments and their relationships to palaeoclimate. Org. Geochem. 29 (5), 1721–1735.
Jiang, Q.G., Wang, Q., Cheng, Q.Q., Zhang, C.M., Liu, W.B., 2005. Discussion on the kinetics characteristics of hydrocarbon generation of different maceral source rocks. Pet. Geol. Exp. 27 (5), 512–533 (In Chinese with English abstract).
Jin, X., Zhang, Z.H., Wu, J., Zhang, C.J., He, Y.N., Cao, L., Zheng, R.H., Meng, W.Q., Xia, H.Y., 2019. Origin and geochemical implication of relatively high abundance of 17α (H)-diahopane in Yabulai basin, Northwest China. Mar. Pet. Geol. 99, 429–442.
Johns, W.D., Shimoyama, A., 1972. Caly minerals and Petroleum-Formation reactions during burial and diagenesis. AAPG Bull. 56, 152–159.
Killops, S., Killops, V., 2005. Introduction to Organic Geochemistry, second ed. Blackwell Publishing, Oxford, pp. 196–203.
Kvalheim, O.M., Christy, A.A., Telnæs, N., Bjørseth, A., 1987. Maturity determination of organic matter in coals using the methylphenanthrene distribution. Geochim. Cosmochim. Acta 51 (7), 1883–1888.
Lai, H.F., Li, M.J., Liu, J.G., Mao, F.J., Xiao, H., He, W.X., Yang, L., 2018. Organic geochemical characteristics and depositional models of Upper cretaceous marine source rocks in the Termit Basin. Niger. Palaeogeography, Palaeoclimatology, Palaeoecology 495, 292–308.
Leushina, E., Mikhaylova, P., Kozlova, E., Polyakov, V., Morozov, N., Spasennykh, M., 2021. The effect of organic matter maturity on kinetics and product distribution during kerogen thermal decomposition: the Bazhenov Formation case study. J. Pet. Sci. Eng. 204, 108751.
Li, Q., Wu, S.H., Xia, D.L., You, X.L., Zhang, H.M., Lu, H., 2020. Major and trace element geochemistry of the lacustrine organic-rich shales from the Upper Triassic Chang 7 Member in the southwestern Ordos Basin, China: Implications for paleoenvironment and organic matter accumulation. Mar. Pet. Geol. 111, 852–867.
Li, W.W., Cao, J., Zhi, D.M., Tang, Y., He, W.J., Wang, T.T., Xia, L.W., 2021a. Controls on shale oil accumulation in alkaline lacustrine settings: late Paleozoic Fengcheng Formation, northwestern Junggar Basin. Mar. Pet. Geol. 129, 105107.
Li, D.L., Shi, Q.M., Mi, N.Z., Xu, Y., Wang, X.K., Tao, W.X., 2021b. The type, origin and preservation of organic matter of the fine-grain sediments in Triassic Yanhe Profile, Ordos Basin, and their relation to paleoenvironment condition. J. Pet. Sci. Eng. 188, 106875.
Lin, S.H., Yuan, X.J., Yang, Z., 2017. Comparative study on lacustrine shale and mudstone and its significance: a case from the 7th member of Yanchang Formation in the Ordos Basin. Oil Gas Geol. 38 (3), 517–523 (In Chinese with English abstract).
Liu, Q., Yuan, X.J., Lin, S.H., Guo, H., Cheng, D.W., 2018. Depositional environment and characteristics comparison between lacustrine mudstone and shale: a case study from the Chang 7 Member of the Yanchang Formation, Ordos Basin. Oil & Gas Geology 39 (3), 531–540 (In Chinese with English abstract).
Liu, M.J., Xiong, T., Xiong, C., Liu, Y., Liu, L., Xiao, D., Tan, X.C., 2020. Evolution of diagenetic system and its controls on the reservoir quality of pre-salt dolostone: the case of the lower Ordovician Majiagou Formation in the Central Ordos Basin, China. Marine and Petroleum Geology 122, 104674.
Mahlstedt, N., Horsfield, B., Dieckmann, V., 2008. Second order reactions as a prelude to gas generation at high maturity. Org. Geochem. 39 (8), 1125–1129.
Mango, F.D., 2000. The origin of light hydrocarbon. Geochimica et Cosmochimical Acta 58, 895–901.
Mao, G.Z., Liu, C.Y., Liu, B.Q., Zhang, D.D., Qiu, X.W., Wang, J.Q., 2012a. Effects of uranium on hydrocarbon generation of low-mature hydrocarbon source rocks containing kerogen type I. Journal of China University of Petroleum (Edition of Natural Science) 36 (2), 172–181 (In Chinese with English abstract).
Mao, G.Z., Liu, C.Y., Zhang, D.D., Qiu, X.W., Wang, J.Q., Liu, B.Q., Liu, J.J., Qu, S.D., Zhang, C., Deng, Y., Wang, F.F., 2012b. Effects of uranium (type II) on evolution of hydrocarbon generation of source rocks. Acta Geol. Sin. 86 (11), 1833–1840 (In Chinese with English abstract).
Mao, G.Z., Liu, C.Y., Zhang, D.D., Qiu, X.W., Wang, J.Q., Liu, B.Q., Liu, J.J., Qu, S.D., Deng, Y., Wang, F.F., Zhang, C., 2014. Effcets of uranium on hydrocarbon generation of hydrocarbon on source rocks with type-III kerogen. Sci. China Earth Sci. 57, 1168–1179 (In Chinese).
Moldowan, J.M., Seifert, W., Gallego, E.J., 1985. Relationship between petroleum composition and depositional environment of petroleum source rocks. AAPG Bull. 69 (8), 1255–1268.
Nytoft, H.P., Lutnaes, B.F., Johansen, J.E., 2006. 28-*Nor*-spergulanes, a novel series of rearranged hopanes. Org. Geochem. 37 (7), 772–786.
Pepper, A.S., Corvit, P.J., 1995. Simple kinetic models of petroleum formation. Part I: oil and gas generation from kerogen. Mar. Pet. Geol. 12 (3), 291–319.
Peters, K.E., Walters, C.C., Moldowan, J.M., 2005. The Biomarker Guide: Column 2, Biomarkers and Isotopes in Petroleum Systems and Earth History, 2nd edition. Cambridge University Press, Cambridge, pp. 48–109.
Philp, R.P., Gilbert, T.D., 1982. Unusual distribution of biological markers in an Australian crude oil. Nature 299, 245–247.
Pickel, W., Kus, J., Flores, D., Kalaitzidis, S., Christanis, K., Cardott, B.J., Misz-Kennan, M., Rodrigues, S., Hentschel, A., Hamor-Video, M., Crosdale, P., Wagner, N., 2017. Classification of liptinite – ICCP System 1994. Int. J. Coal Geol. 169, 40–61.
Püttmann, W., Villar, H., 1987. Occurrence and Geochemical significance of 1,2,5,6-tetramethylnaphthalene. Geochim. Cosmochim. Acta 51 (11), 3023–3029.
Qi, Y.L., Zhang, Z.H., Xia, D.L., Zhang, H.M., Huang, C.X., Zheng, D., Jin, X., Cao, Y.L., Zhu, L., 2019. Comparative analysis of hydrocarbon generation kinetics of dark mudstone and black shale of Chang 7 in southern Ordos Basin. Geoscience 33 (4), 863–871 (In Chinese with English abstract).
Qiao, J.Q., Baniasad, A., Zieger, L., Zhang, C., Luo, Q., Littke, R., 2021. Paleo-depositional environment, origin and characteristics of organic matter of the Triassic Chang 7 Member of the Yanchang Formation throughout the mid-western part of the Ordos Basin. China. International Journal of Coal Geology 237, 103636.
Radke, M., Welte, D.H., 1983. The methylphenanthrene index (MPI): A maturity parameter based on aromatic hydrocarbons. In: Bjorøy, M., Albrecht, C., Cornford, C., et al. (Eds.), Advances in Organic Geochemistry., 10. John Wiley & Sons, New York, USA, pp. 504–512.
Radke, M., Welte, D.H., Willsch, H., 1986. Maturity parameters based on aromatic hydrocarbons: Influence of the organic matter type. Org. Geochem. 10 (1–3), 51–63.
Rimmer, S.M., Thompson, J.A., Goodnight, S.A., Robl, T.L., 2004. Multiple controls on the preservation of organic matter in Devonian–Mississippian marine black shales: geochemical and petrographic evidence. Palaeogeogr. Palaeoclimatol. Palaeoecol. 215 (1–2), 125–154.
Romero-Sarmiento, M.F., Riboulleau, A., Vecoli, M., Laggoun-Défarge, F., Versteegh, G.J. M., 2011. Aliphatic and aromatic biomarkers from Carboniferous coal deposits at Dunbar (East Lothian, Scotland): Palaeobotanical and palaeoenvironmental significance. Palaeogeogr. Palaeoclimatol. Palaeoecol. 309 (3–4), 309–326.
Schenk, H.J., Horsfield, B., 1998. Using natural maturation series to evaluate the utility of parallel reaction kinetics models: an investigation of Toarcian shales and Carboniferous coals, Germany. Organic Geochemistry 29 (1–3), 137–154.
Seewald, J.S., 2003. Organic-inorganic interaction in petroleum-producing sedimentary basins. Nature 426 (20), 327–333.
Soeder, D.J., 2018. The successful development of gas and oil resources from shales in North America. J. Pet. Sci. Eng. 163, 399–420.
Sun, X.G., Wang, G.Y., Jin, K.L., 1999. The kinetic features of hydrocarbon generation of desmocollinite. Chinese Journal of Geology (Scientia Geologica Sinica) 34 (4), 485–491 (In Chinese with English abstract).
Sun, R., Li, Z., Zhao, Z.G., Yang, H.Z., Wang, X.Y., Zhao, Z., 2020. Characteristics and origin of the lower Oligocene marine source rocks controlled by terrigenous organic matter supply in the Baiyun Sag, northern South China Sea. J. Pet. Sci. Eng. 187, 106821.
Tao, S.Z., Wang, C.Y., Du, J.G., Liu, L., Chen, Z., 2015. Geochemical application of tricyclic and tetracyclic terpanes biomarkers in crude oils of NW China. Mar. Pet. Geol. 67, 460–467.
Taylor, G.H., Teichmüller, M., Davis, A., Diessel, C.F.K., Littke, R., Robert, P., 1998. Organic Petrology: Berlin. Gerbrüder Borntraeger, Stuttgart, p. 704.
Tissot, B., 1969. Initial data on the mechanism and Kinetics of oil formation in Sediments; Inst. Fancais Petrole Ann. Rev. Combust. Lipuids 24, 470–501.
Trent, P.V., George, R.H., 2002. Catalysis by mineral surfaces: Implications for Mo Geochemistry in anoxic environments. Geochim. Cosmochim. Acta 66 (21), 3679–3692.
Tyson, R.V., 2001. Sedimentation rate, dilution, preservation and total organic carbon: some results of a modelling study. Org. Geochem. 32 (2), 333–339.
Uguna, C.N., Carr, A.D., Snape, C.E., Meredith, W., Castro-Díaz, M., 2012. A laboratory pyrolysis study on investigate the effect of water pressure on hydrocarbon generation and maturation of coals in geological basins. Org. Geochem. 52, 103–113.
Volkman, J.K., Banks, M.R., Denwer, K., Aquino Neto, F.R., 1989. Biomarker Composition and Depositional Setting of *Tasmanite* Oil Shale from Northern Tasmania, Australia. Presented at the 14th International Meeting on Organic Geochemistry, September 18–22, 1989, Paris.
Wang, M., Lu, S.F., Xue, H.T., 2011. Kinetic simulation of hydrocarbon generation from lacustrine type I kerogen from the Songliao Basin: Model comparison and geological application. Mar. Pet. Geol. 28 (9), 1714–1726.
Wang, F., Zhang, D.J., Xu, G.J., 2017. Additively of hydrocarbon-generation kinetic parameters for organic macerals and its application. Petroleum Exploration and Development 34 (6), 696–701 (in Chinese with English abstract).
Wang, Q.F., Jiang, F.J., Ji, H.C., Jiang, S., Liu, X.H., Zhao, Z., Wu, Y.Q., Xiong, H., Li, Y., Wang, Z., 2020. Effects of paleosedimentary environment on organic matter enrichment in a saline lacustrine rift basin - a case study of Paleogene source rock in the Dongpu Depression, Bohai Bay Basin. J. Pet. Sci. Eng. 195, 107658.
Williams, T.S., Bhattacharya, S., Song, L.S., Vikas, A., Sharma, S., 2021. Petrophysical analysis and mudstone lithofacies classification of the HRZ shale, North Slopem, Alaska. Journal of Petroleum Science and Engineering 109454.
Xi, K.L., Li, K., Cao, Y.C., Lin, M.R., Niu, X.B., Zhu, R.K., Wei, X.Z., You, Y., Liang, X.W., Feng, S.B., 2020. Laminae combination and shale oil enrichment patterns of Chang 7_3 sub-member organic-rich shales in the Triassic Yanchang Formation, Ordos Basin, NW China. Petroleum Exploration and Development 47 (6), 1342–1353.
Xu, J., Zhang, C.M., Xie, X.M., Rui, X.Q., 2018. Separation of macerals in organic-rich source rocks and their geochemical characteristics. Petroleum Geology & Experiment 40 (6), 828–835 (In Chinese with English abstract).
Yang, Y.T., Li, W., Ma, L., 2005. Tectonic and stratigraphic controls of hydrocarbon systems in the Ordos basin: a multicycle cratonic basin in Central China. AAPG Bull. 89 (2), 255–269.

Yang, H., Dou, W.T., Liu, X.Y., Zhang, C.L., 2010. Analysis on sedimentary facies of Member 7 in Yanchang Formation of Triassic in Ordos Basin. Acta Sedimentol. Sin. 28 (2), 254–262 (In Chinese with English abstract).
Yang, H., Niu, X.B., Xu, L.M., Feng, S.B., You, Y., Liang, X.W., Wang, F., Zhang, D.D., 2016. Exploration potential of shale oil in Chang 7 Member, Upper Triassic Yanchang Formation, Ordos Basin, NW China. Petroleum Exploration and Development 43 (4), 560–569.
Yang, Z., Zou, C.N., Wu, S.T., Lin, S.H., Pan, S.Q., Niu, X.B., Men, G.T., Tang, Z.X., Li, G. H., Zhao, J.H., Jia, X.Y., 2019. Formation, distribution and resource potential of the "sweet areas (sections)" of continental shale oil in China. Mar. Pet. Geol. 102, 48–60.
You, J.Y., Liu, Y.Q., Li, Y.J., Zhou, D.W., Zheng, Q.H., Yang, Y.J., Shi, J., Gao, H.F., 2021. Influencing factor of Chang 7 oil shale of Triassic Yanchang Formation in Ordos Basin: Constraint from hydrothermal fluid. J. Pet. Sci. Eng. 201, 108532.
Yu, F.N., Sun, P.C., Zhao, K.A., Ma, L., Tian, X.M., 2019. Experimental constraints on the evolution of organic matter in oil shales during heating: Implications for enhanced in situ oil recovery from oil shales. Fuel 261, 116412.
Zhang, M.Z., Ji, L.M., Wu, Y.D., He, C., 2015. Palynofacies and geochemical analysis of the Triassic Yanchang Formation, Ordos Basin: Implications for hydrocarbon generation potential and the paleoenvironment of continental source rocks. Int. J. Coal Geol. 152, 159–176.
Zhang, W.Z., Yang, W.W., Xie, L.Q., 2017. Controls on organic matter accumulation in the Triassic Chang 7 lacustrine shale of the Ordos Basin, Central China. Int. J. Coal Geol. 183, 38–51.
Zhang, K., Liu, R., Liu, Z.J., Li, B.L., Han, J.B., Zhao, K.A., 2020. Influence of volcanic and hydrothermal activity on organic matter enrichment in the Upper Triassic Yanchang Formation, southern Ordos Basin, Central China. Marine and Petroleum Geology 112, 104059.
Zhao, J.F., Mountney, N.P., Liu, C.Y., Qu, H.J., Lin, J.Y., 2015. Outcrop architecture of a fluvio-lacustrine succession: Upper Triassic Yanchang Formation, Ordos Basin, China. Mar. Pet. Geol. 68, 394–413.
Zhao, W.Z., Zhu, R.K., Hu, S.Y., Hou, L.H., 2020. Accumulation contribution differences between lacustrine organic-rich shales and mudstones and their significance in shale oil evaluation. Pet. Explor. Dev. 47 (6), 1160–1171.
Zhao, B.S., Li, R.X., Qin, X.L., Wang, N., Zhou, W., Khaled, A., Zhao, D., Zhang, Y.N., Wu, X.L., Liu, Q., 2021. Geochemical characteristics and mechanism of organic matter accumulation of marine-continental transitional shale of the lower Permian Shanxi Formation, southeastern Ordos Basin, North China. J. Pet. Sci. Eng. 205, 108815.